Supporting Information

Exploring the effect of a pendent amine group poised over the secondary coordination sphere of a cobalt complex on the electrocatalytic hydrogen evolution reaction

Afsar Ali[a#], Rajaneesh Kumar Verma[a#], Avijit Das,[a] Sayantan Paria*

[a]Department of Chemistry, Indian Institute of Technology Delhi, Hauz Khas, New Delhi 110016, India
# Equally contributed

E-mail: sparia@chemistry.iitd.ac.in

General. All the chemicals used in this study were purchased from commercial sources and used as received unless otherwise noted. Solvents were dried according to literature procedures. Methanol and ethanol were dried over metallic magnesium. Acetonitrile and dichloromethane were dried over calcium hydride. Caution: *Although no problems were encountered during the synthesis of the complex, perchlorate salts are potentially explosive and should be handled with care*![1]

The Fourier transform infrared spectrum of the Co complexes was determined on a KBr pellet in a Nicolet protégé 460 ESP instrument. Elemental analysis of **2** was performed in a PerkinElmer 2400 Series II CHNS/O instrument. ESI-mass data of **2** was measured in a Waters Xevo-G2XQTOF instrument. GC data for the quantification of H_2 was measured in an Agilent 7890B GC system fitted with a TCD detector. The ^{1}H-NMR spectra of the ligand and Co complex were recorded in a Bruker 500 MHz (DPX-500) NMR instrument. The UV-vis spectra of the Co complexes were measured in an Agilent 8454 Diode-array spectrophotometer. FE-SEM and EDX data were obtained using a FEI Quanta 200F integrated with an Oxford-EDS system IE 250 X Max 80, Netherlands instrument. The quantification of generated H_2 after the CPE experiment was measured by using an Agilent 7890B gas chromatography instrument fitted with a TCD detector.

Electrochemistry. Cyclic voltammetry (CV) and differential pulse voltammetry (DPV) data of the Co complexes were measured in a CH Instrument (CHI 760E, CH Instrument, USA) using a glassy carbon (ID: 3 mm diameter) as working electrode (WE), Pt wire as a counter electrode (CE), and Ag/AgCl (in saturated KCl) as the reference electrode. $E_{1/2}$ value of the Co^{III}/Co^{II} couple of **1** and **2** were obtained from the CV or from the DPV data using the following expression:

$$E_p = E_{1/2} - 1/2\Delta E \text{ (S1)}$$

Where E_p is the peak potential in a DPV scan, and ΔE is the variation of potential in each DPV step.

In a CV or DPV experiment, 1 mM complex solution in a deoxygenated buffer solution containing 100 mM sodium sulfate was prepared, and data were collected at 25 °C.

Diffusion Coefficient Calculations for $Co^{III/II}$:

Diffusion coefficient (D) for the Co complexes (**1 and 2**) were determined using the on the Randles–Ševčík equation (S2):

$$i_{redox} = 0.446 \, n^{3/2} \, A \, C_{Cat} \, (vF^3D/RT)^{1/2} \text{ (S2)}$$

Where, i_{redox} = Reduction peak current of the Co^{III}/Co^{II} redox couple under N_2. n =1 is the number of electrons transferred in the redox process. C = concentration of catalyst (10×10^{-7} mole/cm^3, 1 mM), F= 96485 C/mol, Faraday constant. A= 0.0707 cm^2 surface area of glassy carbon working electrode. T= 298 K, R= ideal gas constant (8.314 J/K). The value of D was obtained from the slope of a plot of i_{redox} vs. $v1/2$, where the expression of the slope is given in eq S3. has been calculated for the Co^{III}/Co^{II} redox peak by measuring of slope at variable scan rate in 0.1 M PBS for **1** and **2** at pH 4 and 7.

$$Slope = \left(\frac{ip}{\sqrt{v}}\right) = k.\,n^{\frac{3}{2}}.\,A.\,\sqrt{D}\,.C \qquad \text{........(S3)}$$

Where, $k = 2.69 \times 10^5$ C mol^{-1} V$^{-1/2}$, n = 1, A = 0.0707 cm^2

C = 10.0×10^{-7} mole/cm^3 and slope for 1 at pH 4 = 1.02×10^{-5}, slope for 1 at pH 7 = 1.70×10^{-5}, slope for **2** at pH 4 = 1.02×10^{-5}, and slope for **2** at pH 7 = 1.00×10^{-5}

After putting all values in equation S3, we calculated the diffusion coefficient values as follows:

For **1** at

pH 4: 2.80×10^{-5} cm^2 s^{-1}

pH 7:n 7.90×10^{-5} cm^2 s^{-1}.

For **2** at

pH 4: 2.80×10^{-5} cm^2 s^{-1}

pH 7: 2.70×10^{-5} cm^2 s^{-1}

A constant potential electrolysis experiment was performed in an H-type cell separated by a glass frit. One side of the cell was fitted with a plastic chip working electrode (1×1 cm^2) and the Ag/AgCl (in saturated KCl) reference electrode, while the other side with a plastic chip counter electrode (3×1 cm^2). In a typical experiment, one side of the cell (fitted with WE) was filled with 0.1 M PBS containing the complex, and the other side (fitted with CE) with an equal volume of the buffer solution without the catalyst, and the cell was sealed with septa. Constant potential electrolysis (CPE) was performed at a suitable potential. After the CPE, the head space of the H-type cell (containing the WE) was analyzed by GC technique equipped with a TCD detector.

We determined the Faradaic efficiency of **1** and **2** in 0.1 M PBS at pH 7 and 4 using the following formula.

$$Faradaic\ Efficiency = \frac{n \cdot F \cdot N}{Q} \times 100$$

Here, N is the amount of product formed, and Q is the total charge passed.

The turnover number for the HER was calculated using the following formula:

TON = Amount of hydrogen produced (moles)/Amount of catalysts used (moles)

X-ray Crystallography. Single crystals of Co^{II} Complex (**2a**), suitable for X-ray diffraction, were obtained by diffusing diethyl ether into the acetonitrile solution of the complex at room temperature. Crystal data was measured on a Bruker D8 VENTURE Microfocus diffractometer system equipped with a PHOTON II Detector, with Mo K$_\alpha$ radiation (λ = 0.71073 Å) and controlled by the APEX4 (v2022.1−1) software package. The raw data were integrated and corrected for Lorentz and polarization effects with the aid of the Bruker APEX4 program suite. Absorption corrections were performed by using SADABS. Structures were solved by the

intrinsic phasing method and refined against all data in the reported 2θ ranges by the full-matrix least squares method based on F^2 using the SHELXL program suite[2] with all observed reflections. Hydrogen atoms at idealized positions were included in the final refinements. The non-hydrogen atoms were treated anisotropically. Diagrams for the complexes were prepared using Mercury software.[3] Crystallographic data of the complex is given in Table S1, and bond parameters are mentioned in Table S2. CCDC number of the Co[II] structure is 2322859.

Table S1. Crystallographic parameters of **2a**.

Identification code	**2a**
Empirical formula	$C_{24}H_{27}N_7O_{10}Cl_2Co$
Formula weight	703.35
Temperature/K	100.00
Crystal system	monoclinic
Space group	$P2_1/c$
a/Å	22.7738(14)
b/Å	8.1597(5)
c/Å	15.4972(8)
α/°	90
β/°	93.142(2)
γ/°	90
Volume/Å^3	2875.5(3)
Z	4
ρcalcg/cm^3	1.625
μ/mm^{-1}	0.851
F(000)	1444.0
Radiation	MoKα (λ = 0.71073)
2Θ range for data collection/°	3.582 to 56.7
Index ranges	$-30 \leq h \leq 30, -10 \leq k \leq 10, -20 \leq l \leq 20$
Reflections collected	60228
Independent reflections	7153 [Rint = 0.0760, Rsigma = 0.0416]
Data/restraints/parameters	7153/0/405
Goodness-of-fit on F^2	1.131
Final R indexes [I>=2σ (I)]	R1 = 0.0644, wR2 = 0.1556
Final R indexes [all data]	R1 = 0.0735, wR2 = 0.1612
Largest diff. peak/hole / e Å^{-3}	0.95/−0.95

Table S2. Selected bond lengths and bond angles of **2a**.

Bonding Interactions	Bond length (Å)
Co(1)−N(2)	1.887
Co(1)−N(3)	1.891
Co(1)−N(4)	1.887
Co(1)−N(5)	1.890
Co(1)−N(7)	2.130
Bonding Interactions	Bond Angle (º)
N(2)−Co(1)−N(3)	96.60 (12)
N(2)−Co(1)−N(5)	83.82 (12)
N(3)−Co(1)−N(4)	84.13 (13)
N(4)−Co(1)−N(5)	96.83 (13)
N(2)−Co(1)−N(7)	93.23 (12)
N(3)−Co(1)−N(7)	96.74 (12)
N(4)−Co(1)−N(7)	92.05 (12)
N(5)−Co(1)−N(7)	90.07 (12)
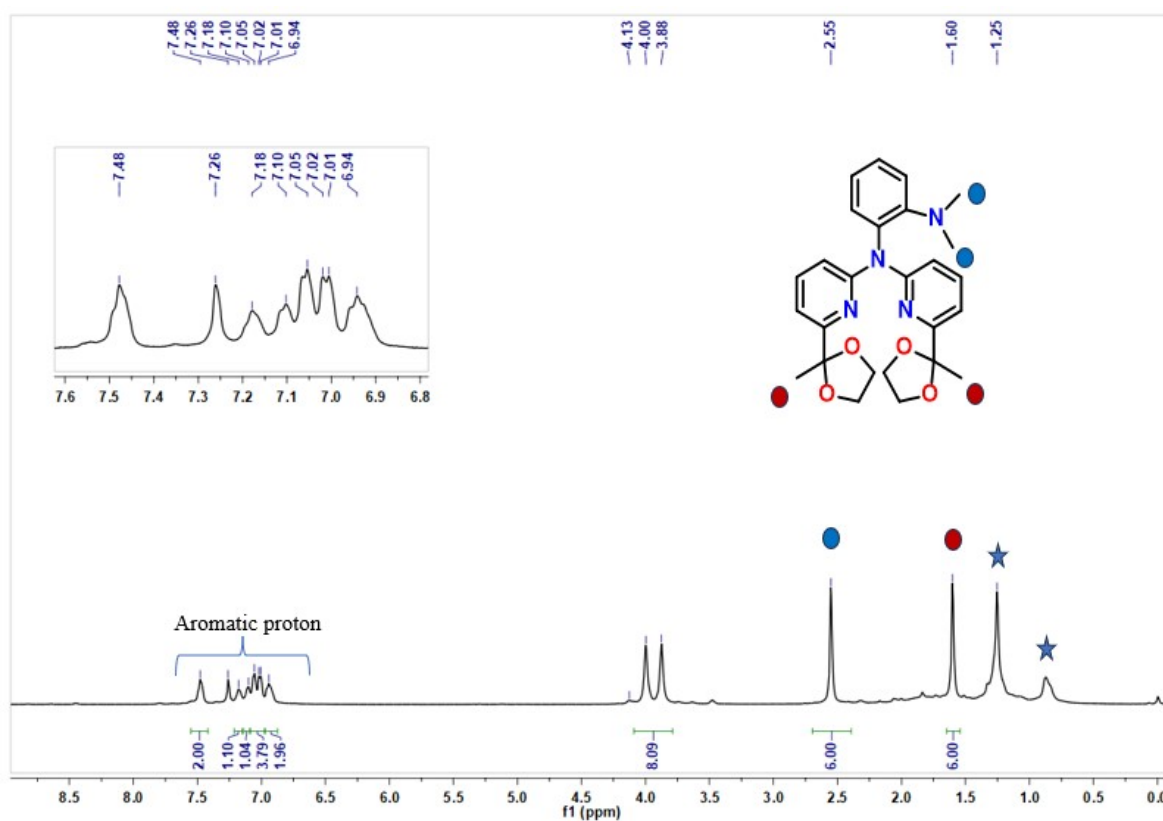
Figure S1. The ^{1}H-NMR spectrum (CDCl$_3$, 500 MHz, 25 °C) of N^1,N^1-dimethyl-N^2,N^2-bis(6-(2-methyl-1,3-dioxolan-2-yl)pyridin-2-yl)benzene-1,2-diamine (**P3**).
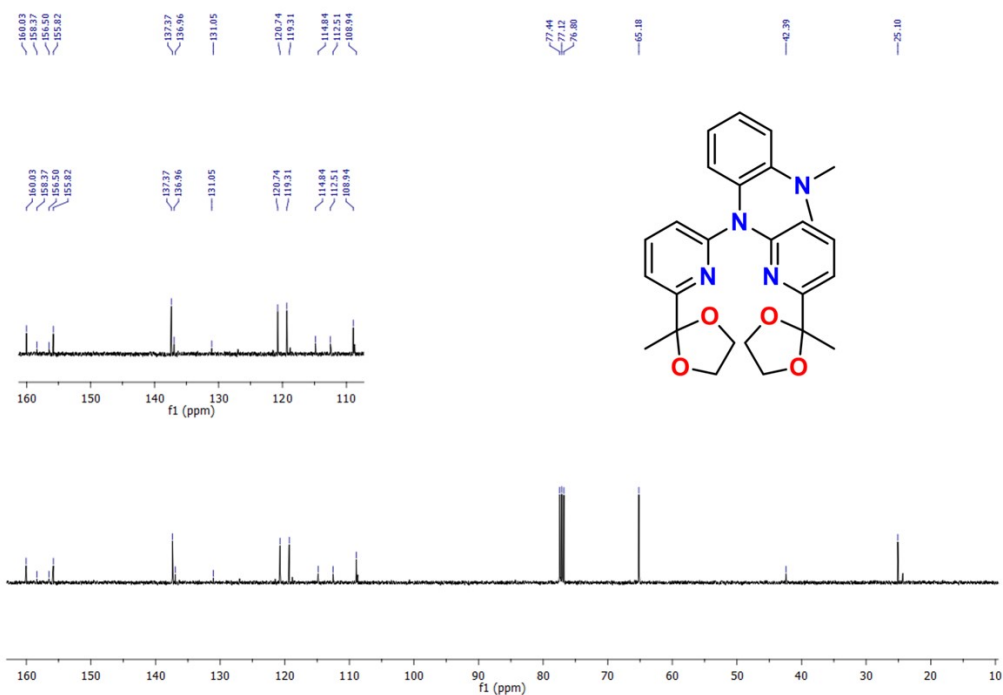
Figure S2. ^{13}C NMR (125 MHz, CDCl$_3$, 25 °C) spectrum of **P3**.
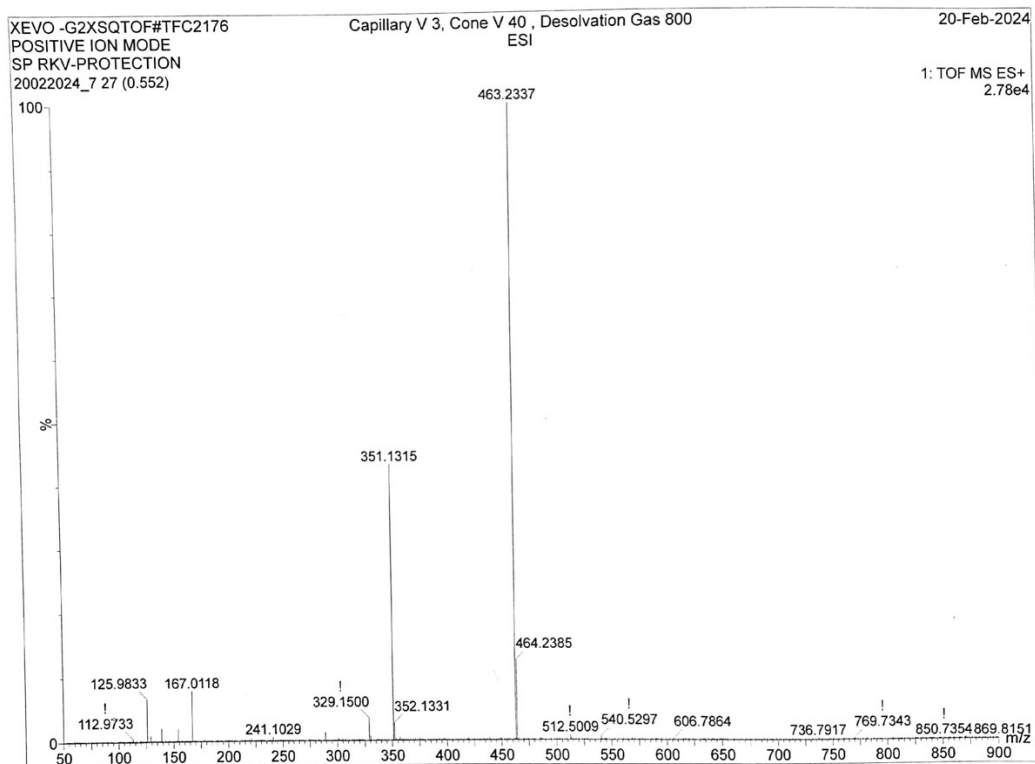
Figure S3. The ESI-mass spectrum of **P3** in methanol (positive ion mode).
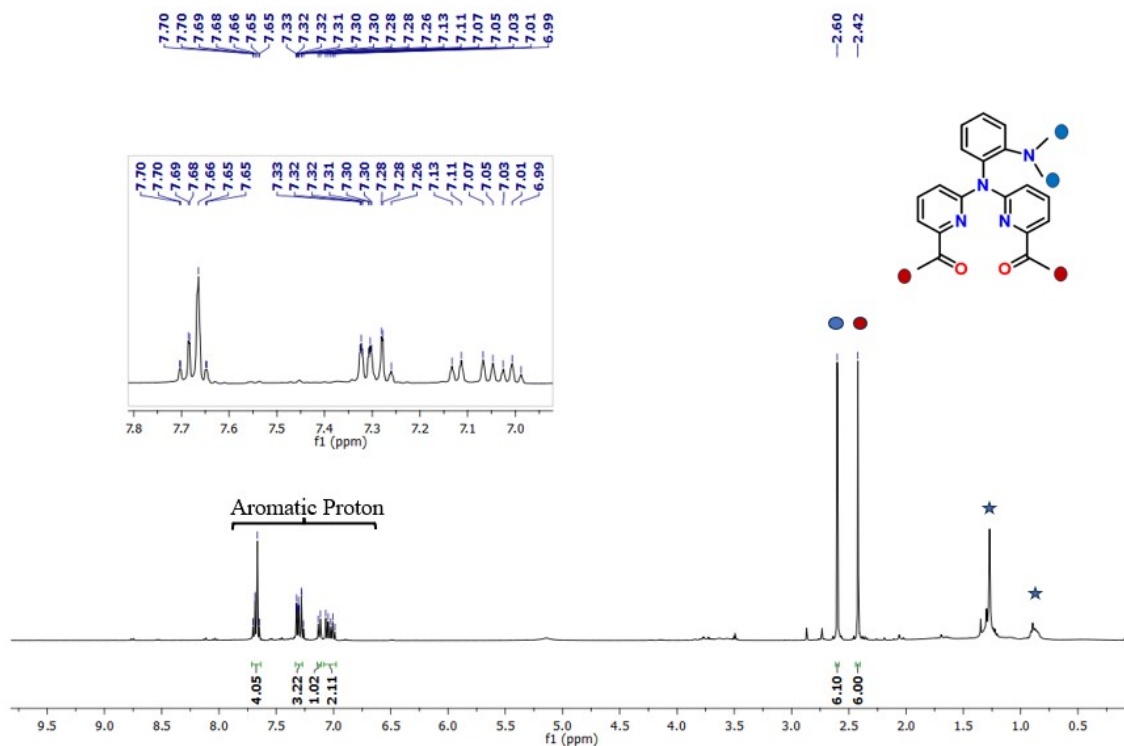
Figure S4. The ¹H NMR spectrum (CDCl₃, 500 MHz, 25 °C) of 1,1'-(((2-(dimethylamino)phenyl)azanediyl)bis(pyridine-6,2-diyl))bis(ethan-1-one) (**P4**).
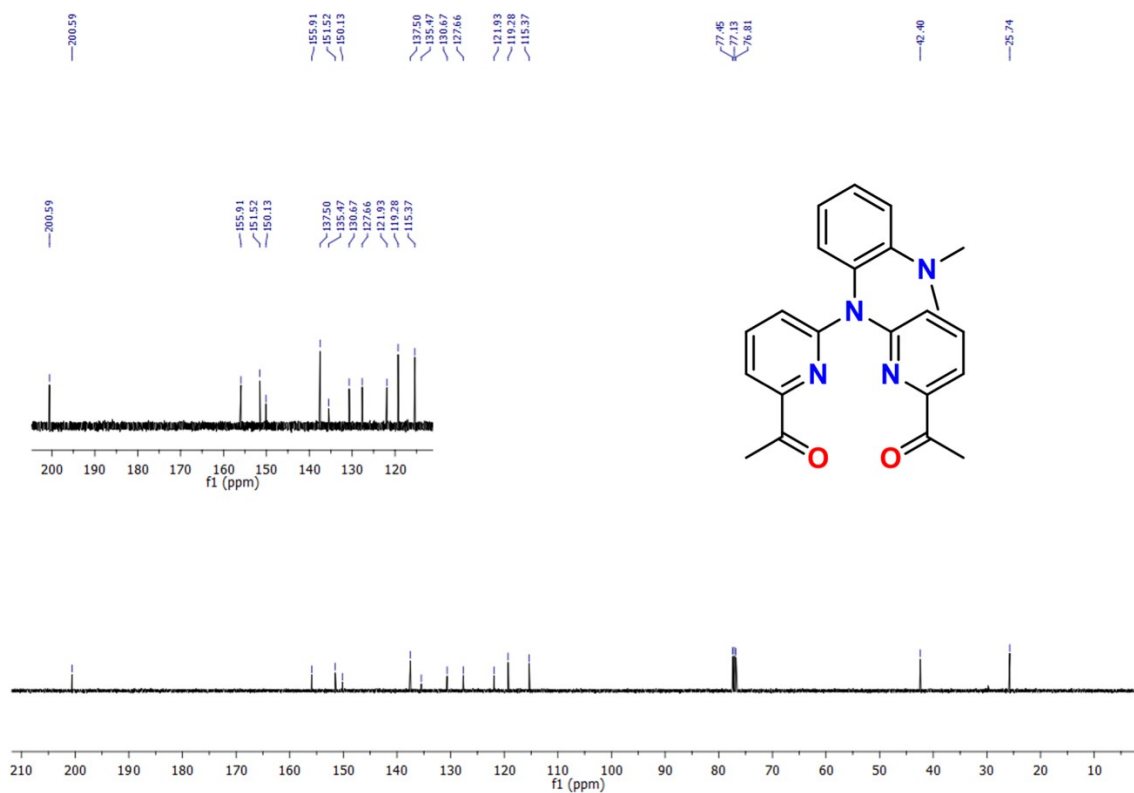
Figure S5. ¹³C NMR (125 MHz, CDCl₃, 25 °C) spectrum of **P4**.
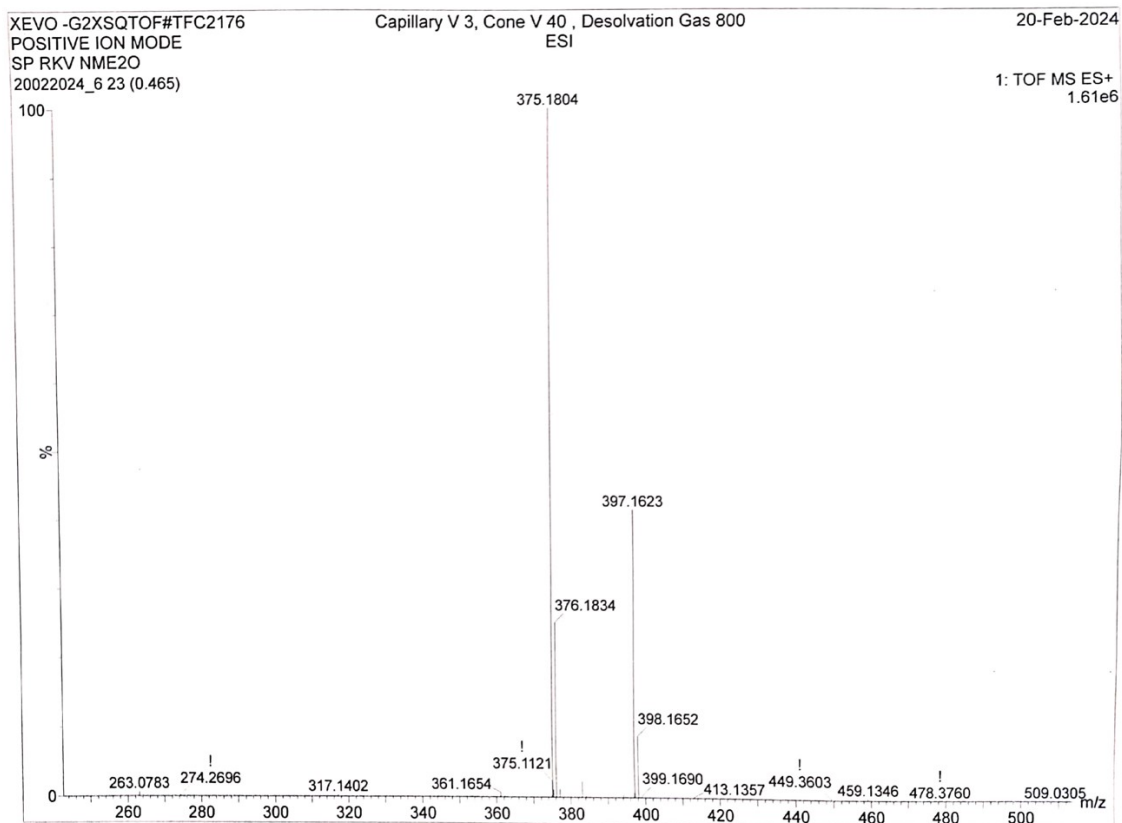
Figure S6. ESI mass spectrum (positive ion mode) of **P4** in methanol.
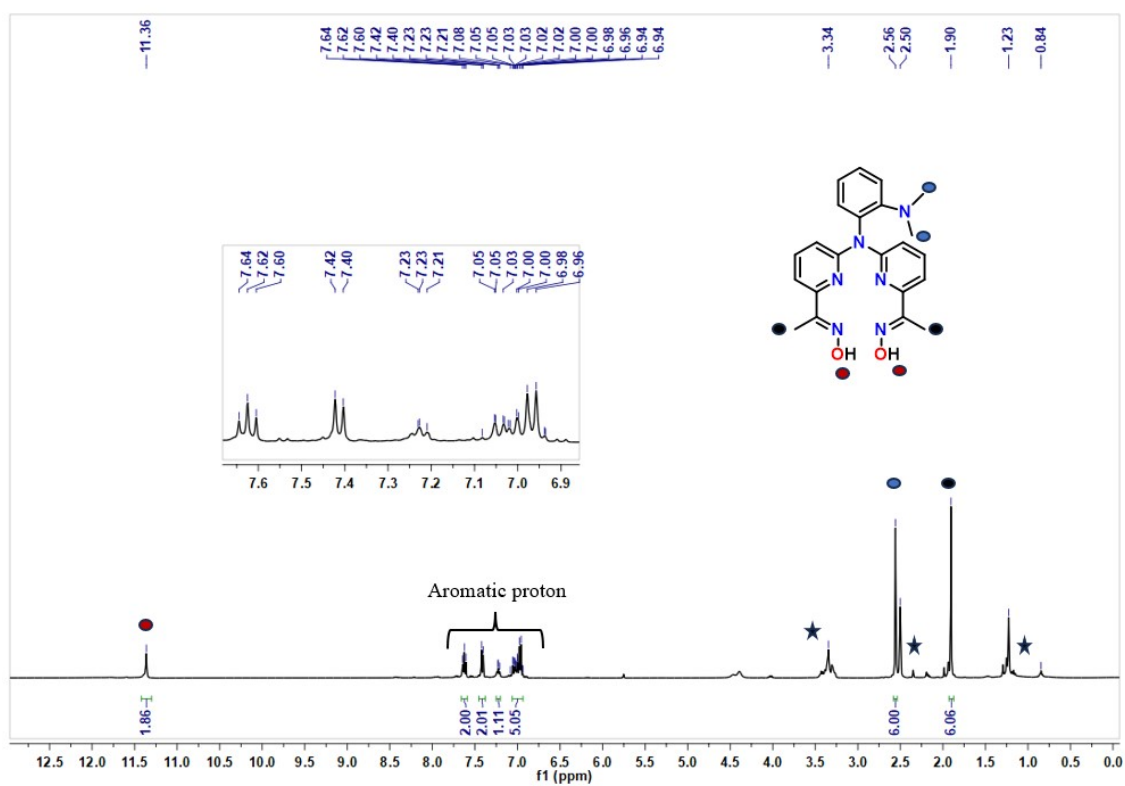
Figure S7. ^{1}H-NMR spectrum of H_2L^{NMe2} (DMSO-d_6, 500 MHz, 25 °C).
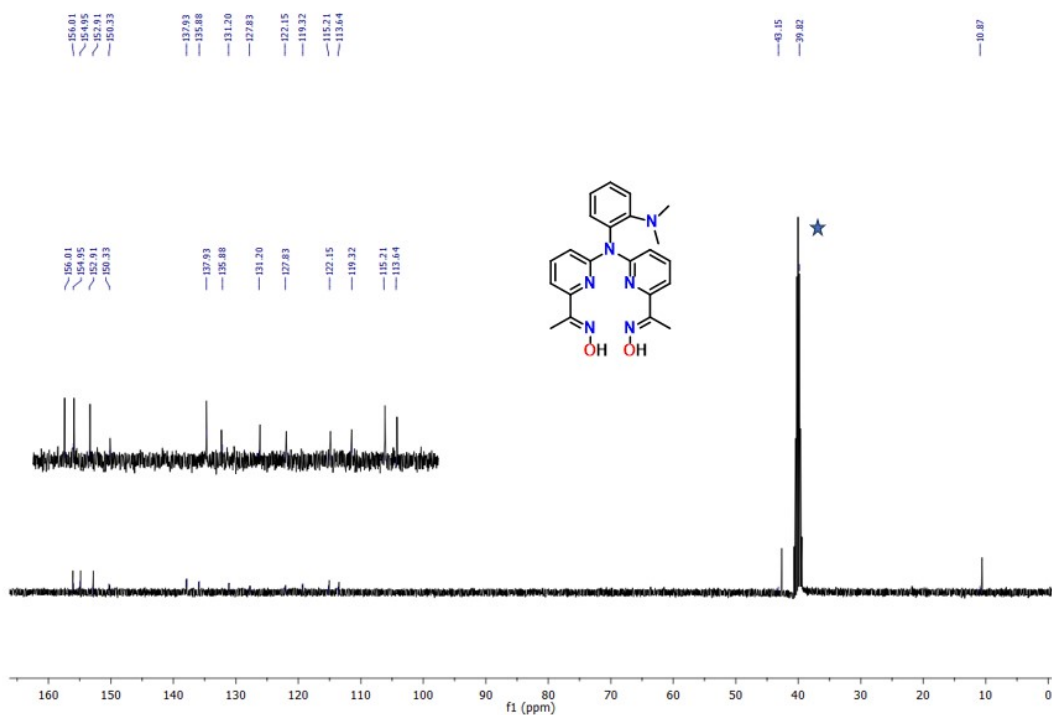
Figure S8. ^{13}C-NMR spectrum (125 MHz, DMSO-d_6, 25 °C) of H$_2$L^{NMe2} in.
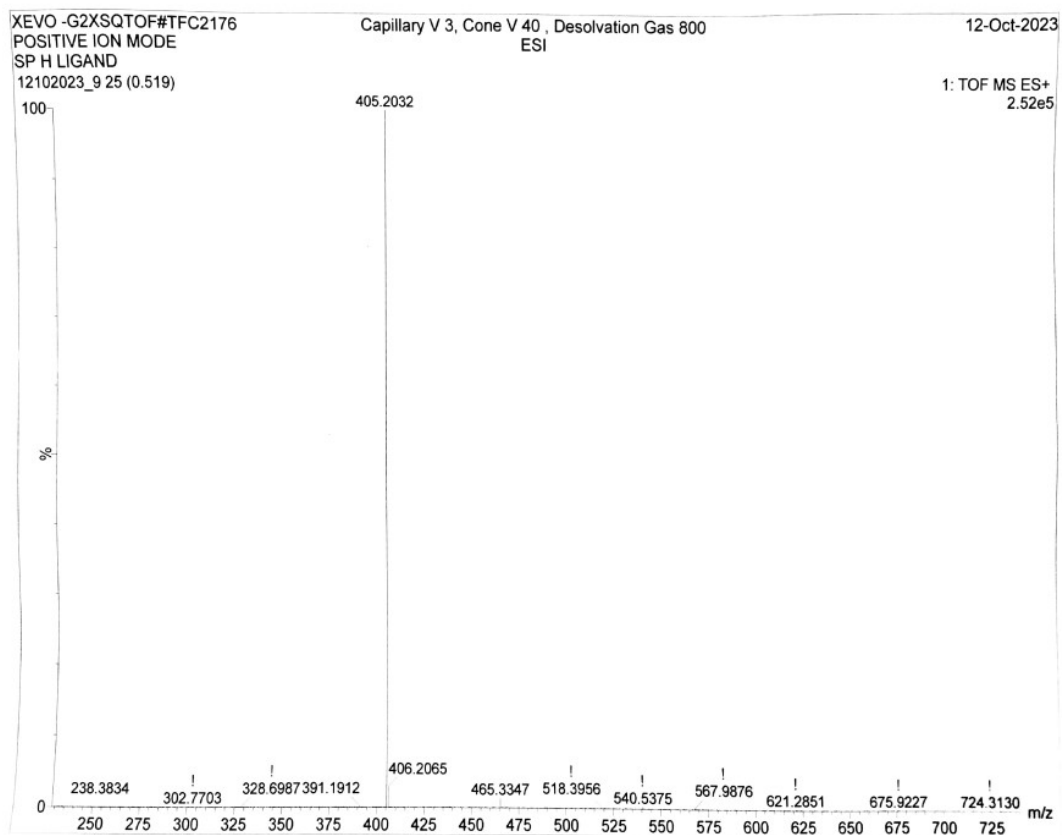
Figure S9. The ESI-mass spectrum of H$_2$L^{NMe2} in methanol.
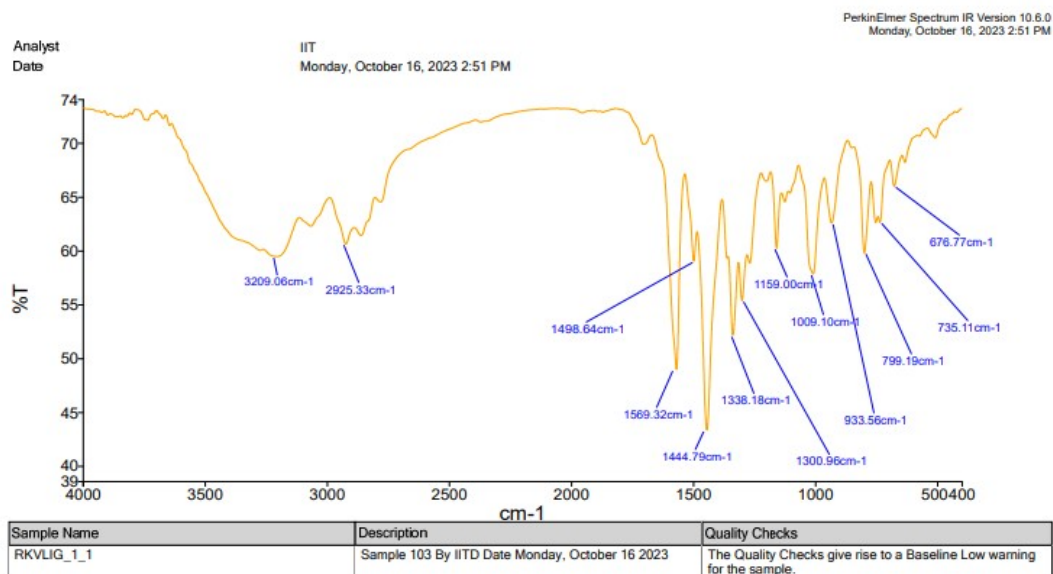
Figure S10. FT-IR spectrum of H_2L^{NMe2}, recorded on KBr pellet.
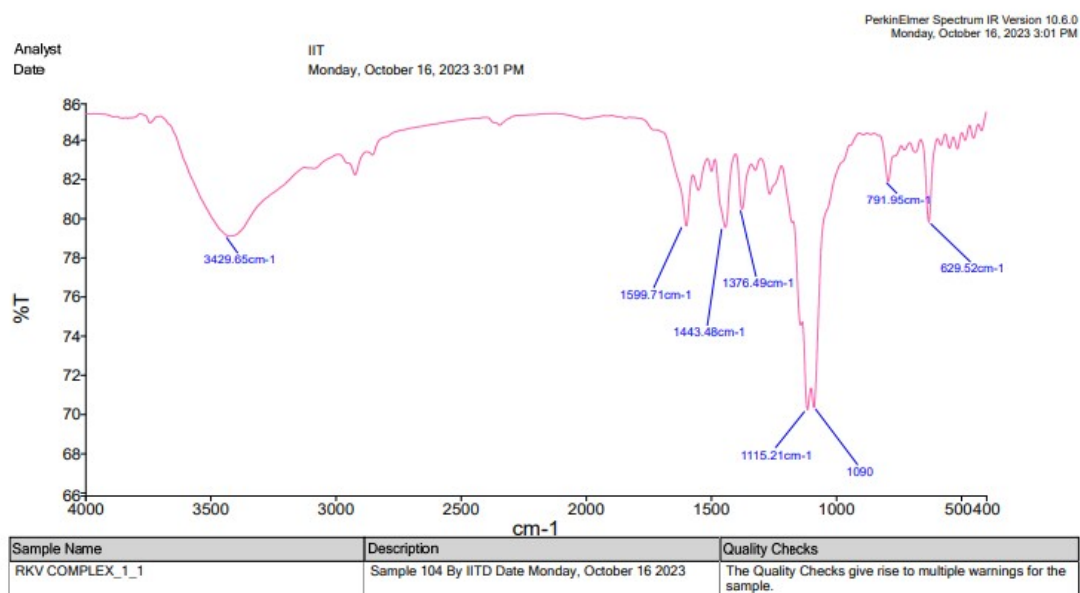
Figure S11. FT-IR spectrum of **2**, recorded on KBr pellet.
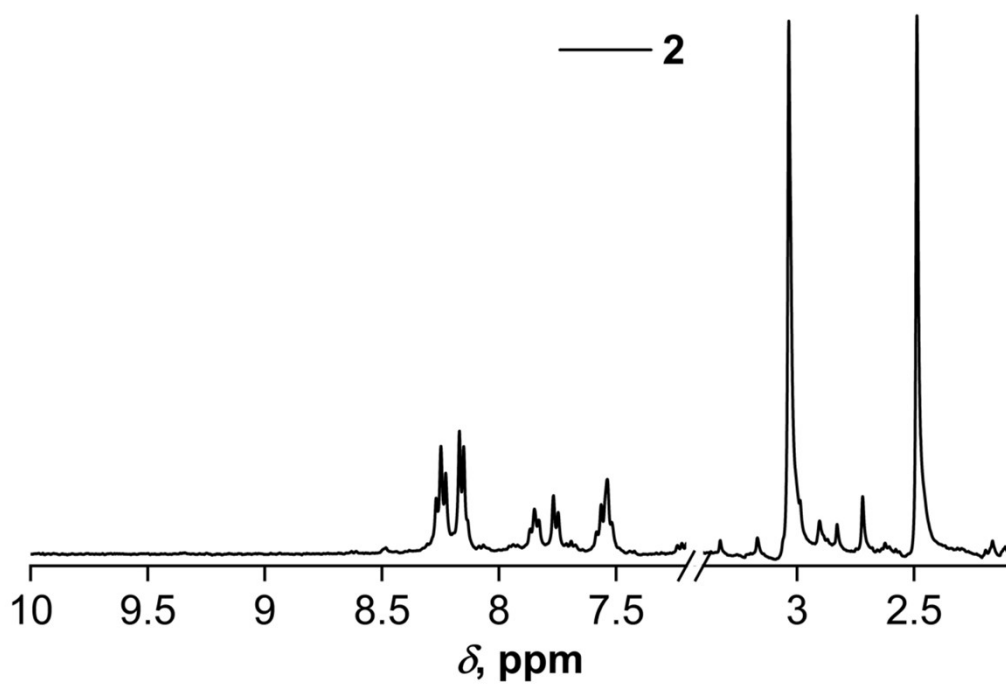
Figure S12. ^{1}H NMR of **2** (500 MHz, D$_2$O, 25 °C).
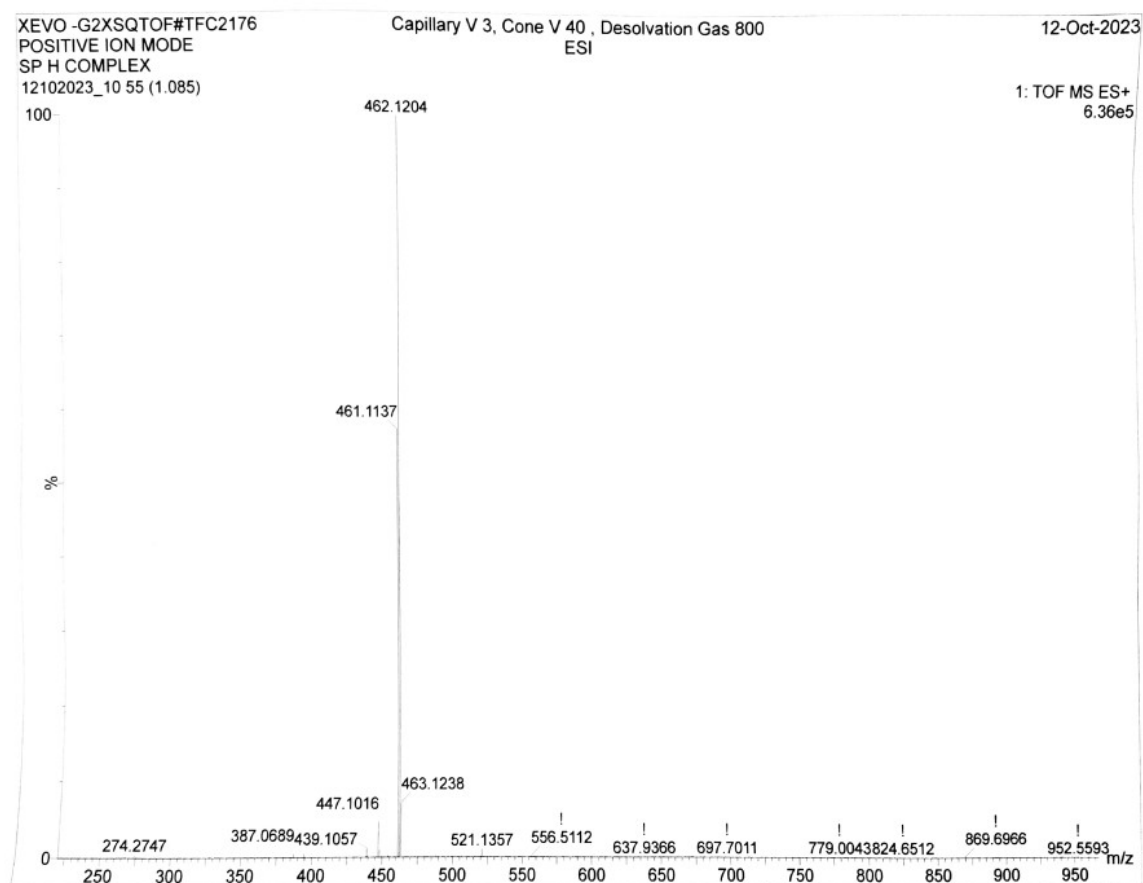
Figure S13. The ESI-mass spectrum of **2**, measured in methanol.
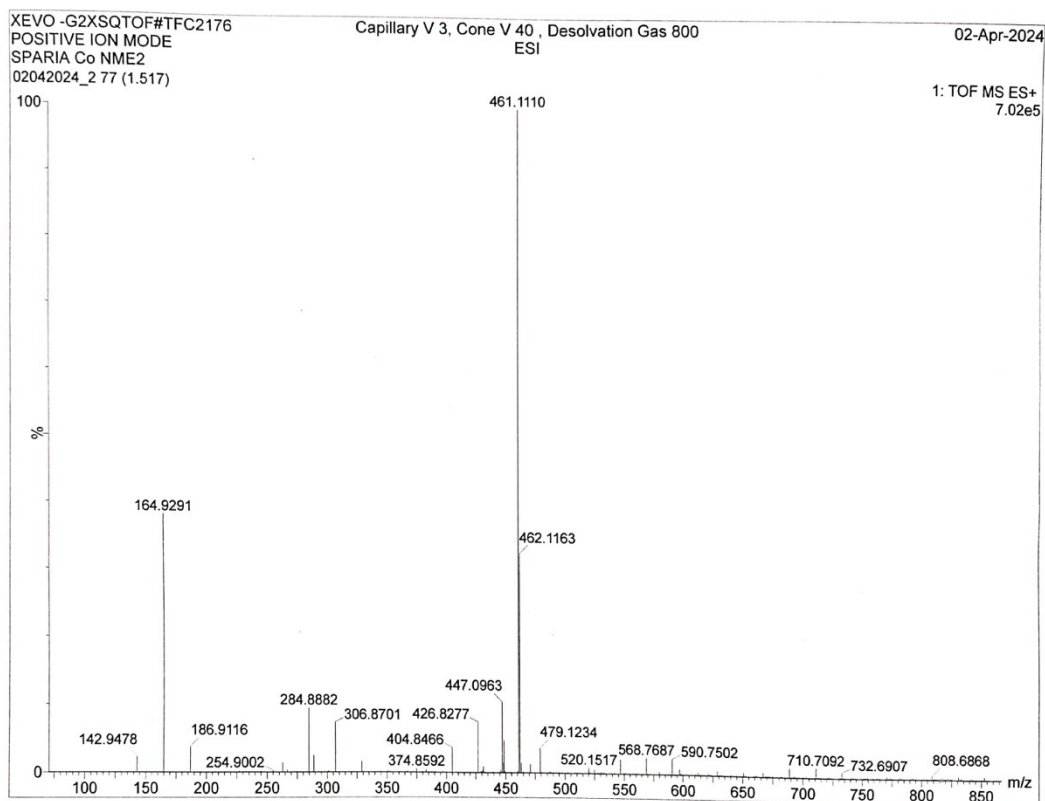
Figure S14. The ESI-mass spectrum of **2** measured in 0.1 M PBS.
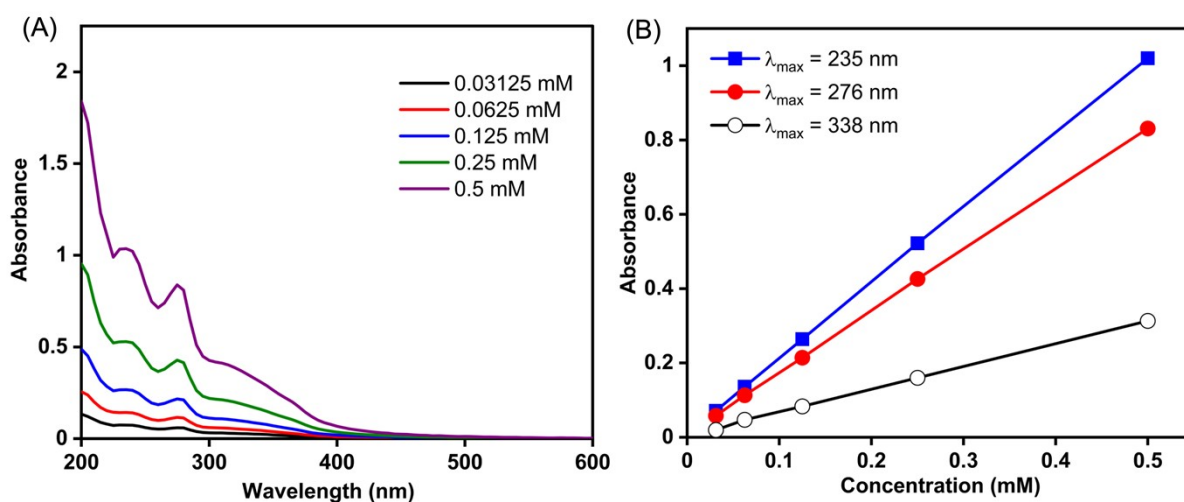
Figure S15. (A) UV-vis spectrum of **2** in a 0.1 M PBS, measured using different concentrations using a 0.1 cm pathlength cuvette. (B) A plot of absorbance vs. complex concentration for the estimation of molar extinction coefficient at different absorbance maxima.
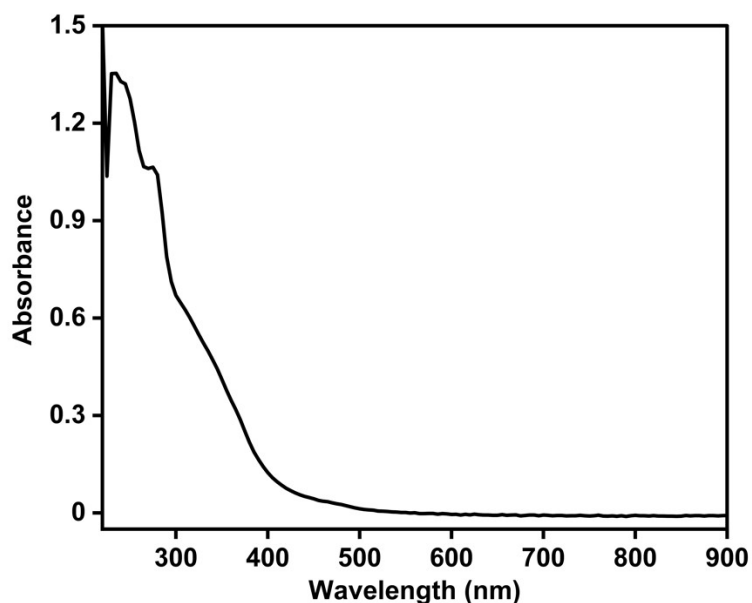
Figure S16. UV-vis spectrum of **2** (0.25 mM) in methanol at 25 °C. The data was measured using a 1 cm pathlength cuvette.
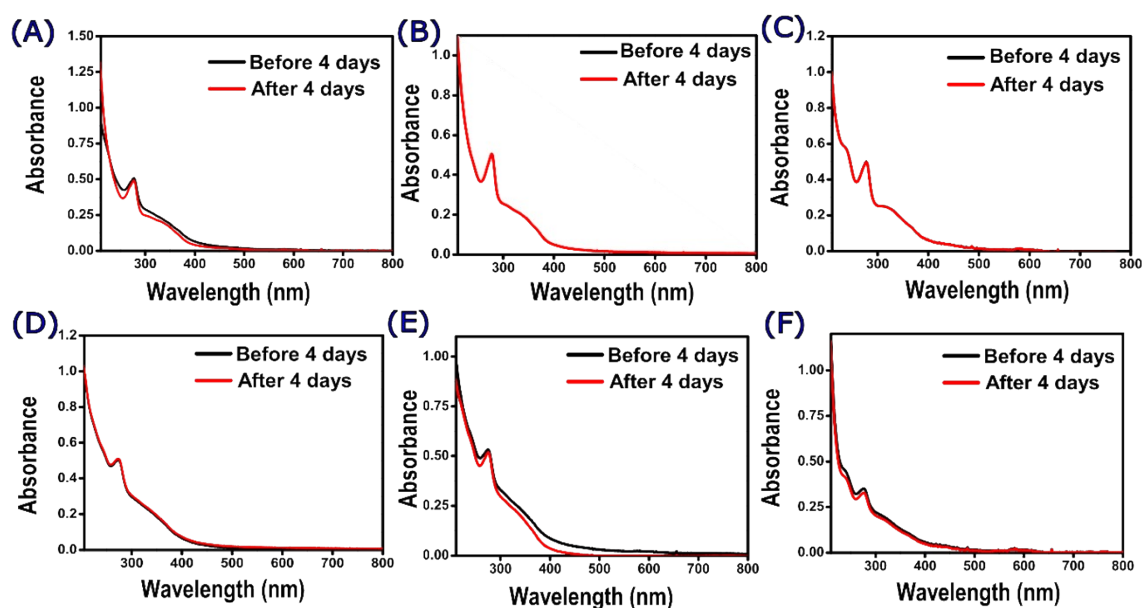
Figure S17. UV-vis spectra for **1** (0.5 mM, black trace) in 0.1 M PBS at pH 2.5 (A), pH 4 (B), and pH 7 (C). The red trace denotes the spectrum of the same complex solution measured after 4 days. UV spectra for **2** (0.5 mM, black trace) in 0.1 M PBS at pH 2.5 (D), pH 4 (E), and pH 7 (F). The red trace denotes the spectrum of the same complex solution measured after 4 days.

Slightly degradation (3-4 %) of complexes **1** and **2** were observed in 0.1 M PBS at pH 2.5 and 4. The UV-vis spectra described here were recorded using a 1 cm pathlength cuvette.
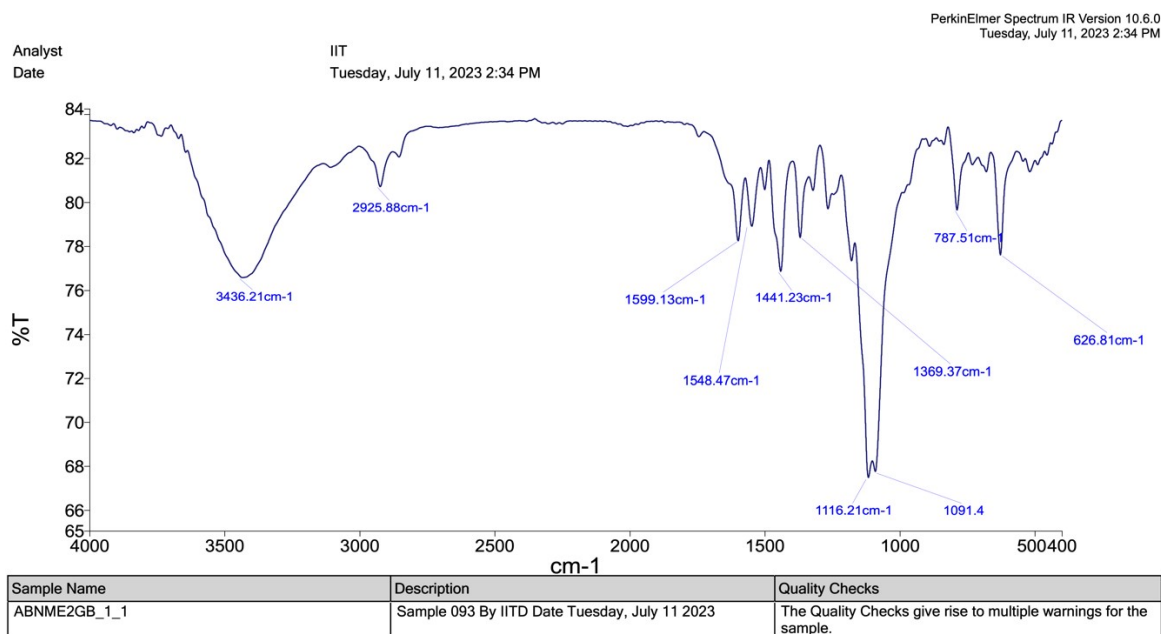
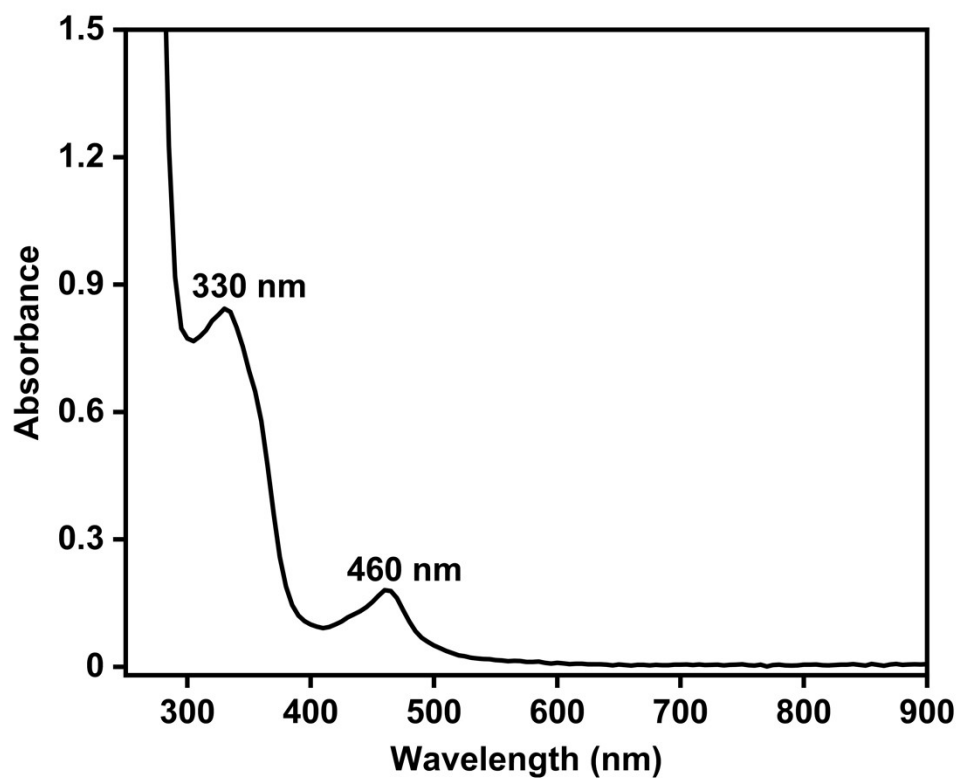**Figure S18**. FT-IR spectrum of **2a**, measured on KBr pellet.

Figure S19. UV-vis spectrum of **2a** (0.5 mM) in 0.1 M PBS at pH 7.0. The data was recorded using a 1 cm pathlength cuvette.
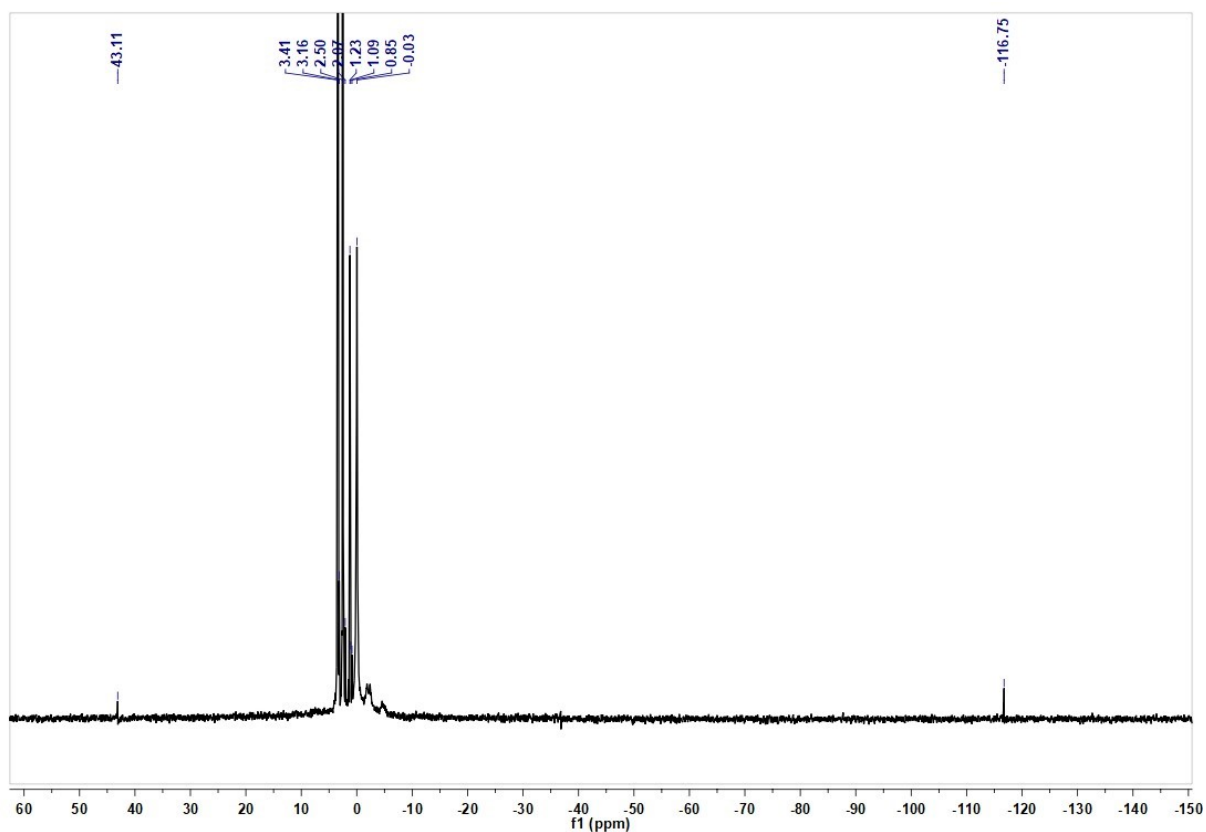
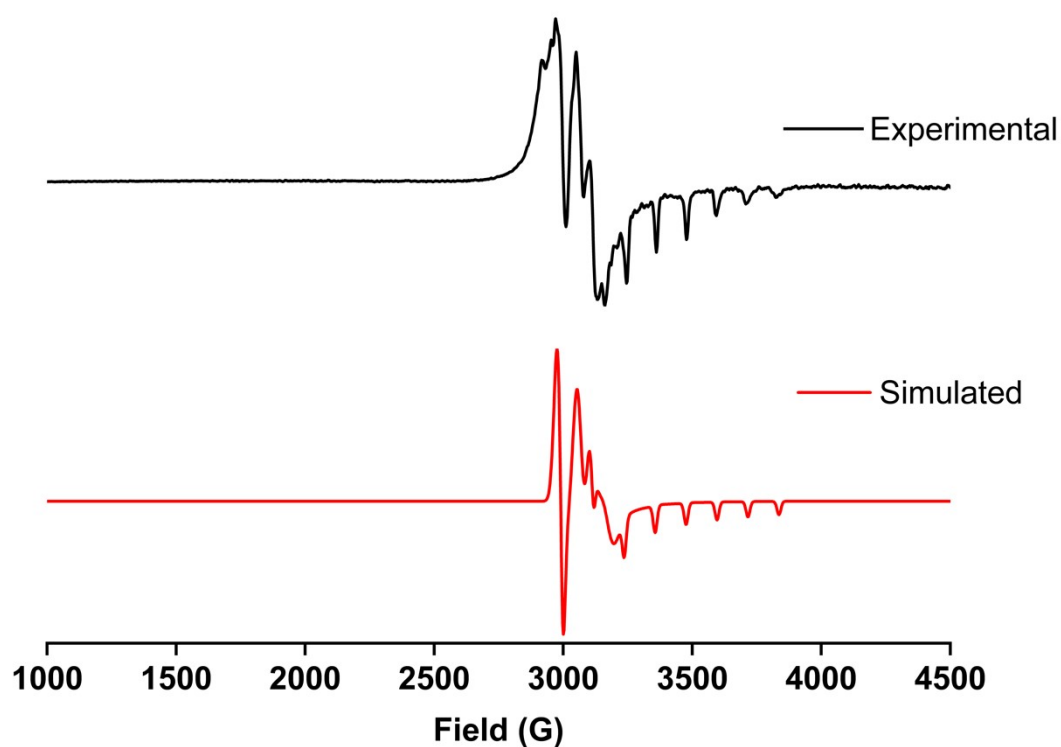**Figure S20**. ^{1}H NMR spectrum of **2a** (DMSO-d_6, 500 MHz, 25 °C).

Figure S21. Experimental and simulated X-band EPR spectra of **2a** in frozen methanol at 77 K. Simulated parameters: $g_x = 2.19$, $g_y = 2.085$ and $g_z = 2.015$, $A_{xx}^{Co} = 10$ G, $A_{yy}^{Co} = 20$ G, $A_{zz}^{Co} = 120$ G. Experimental conditions: Power = 3.51 mW, Frequency = 9.6328 GHz, Modulation frequency = 100 kHz, Modulation amplitude = 4.91 G.
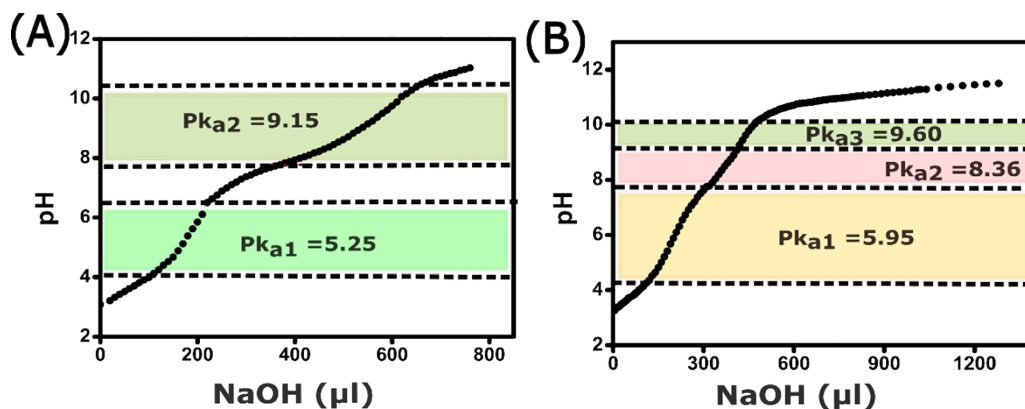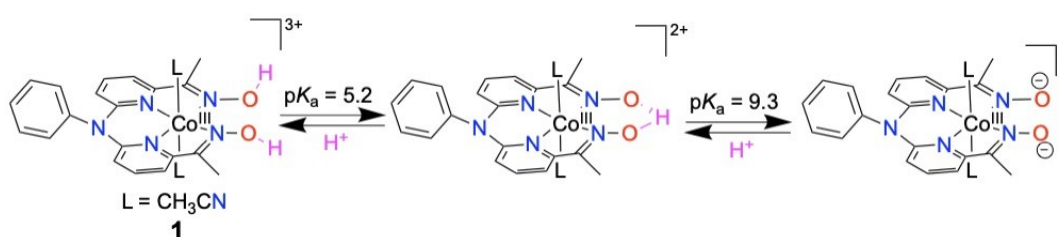
Figure S22. pH titration for complex **1** (1 mM) and **2** (1 mM) in aqueous solution by the incremental addition of aqueous NaOH (25 mM) at 25 °C.

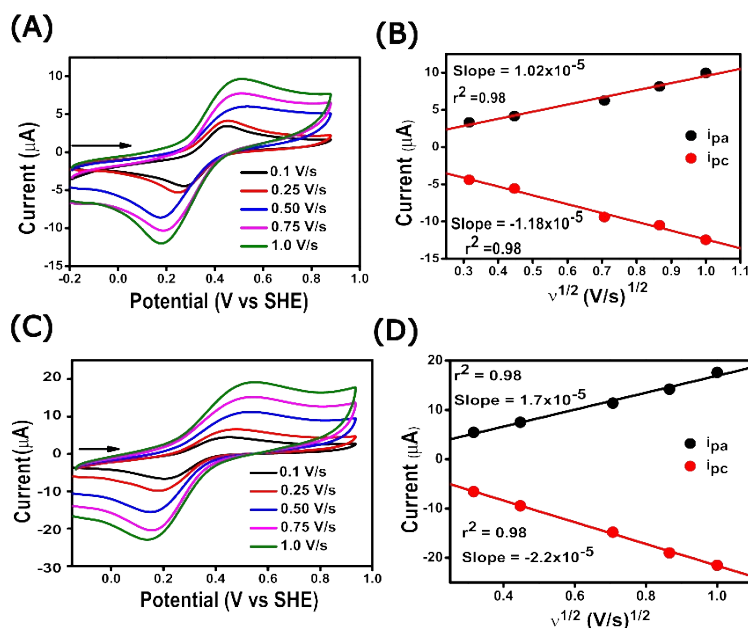**Scheme S1.** Acid-base properties of **1** in 0.1 M PBS.

Figure S23. (A) $Co^{III/II}$ redox couple of **1** (1 mM) measured in PBS (pH 4) at variable scan rates. (B) Linear dependency of the current (μA) vs. square root of scan rate ($v^{1/2}$). (C) $Co^{III/II}$ redox couple of **1** (1 mM) measured in PBS (pH 7) at variable scan rate. (D) Linear dependency of current (μA) vs. square root of scan rate ($v^{1/2}$). The data were recorded using a 3 mm diameter glassy carbon disc working electrode, Pt wire counter electrode, and Ag/AgCl (in saturated KCl) reference electrode under N_2 atmosphere.
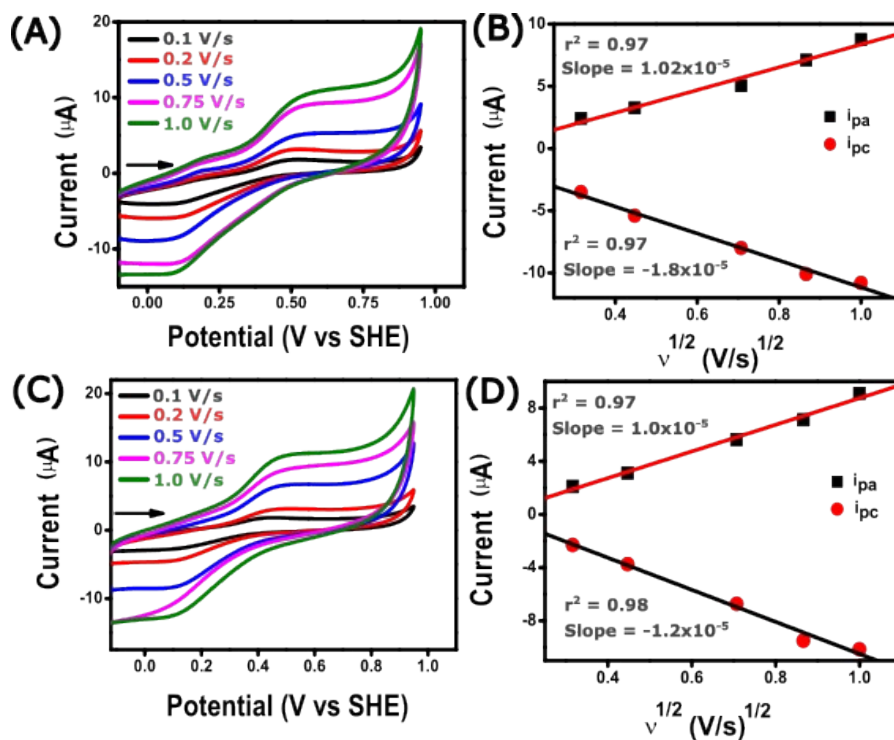
Figure S24. (A) $Co^{III/II}$ redox couple of **2** (1 mM) measured in PBS (pH 4) at variable scan rates. (B) Linear dependency of current (μA) vs. square root of scan rate ($v^{1/2}$). (C) $Co^{III/II}$ redox couple of **2** (1 mM) measured in PBS (pH 7) at variable scan rates. (D) Linear dependency of current (μA) vs. square root of scan rate ($v^{1/2}$). The data was recorded using a 3 mm diameter glassy carbon disc working electrode, Pt wire counter electrode, and Ag/AgCl (in saturated KCl) reference electrode under N_2 atmosphere.
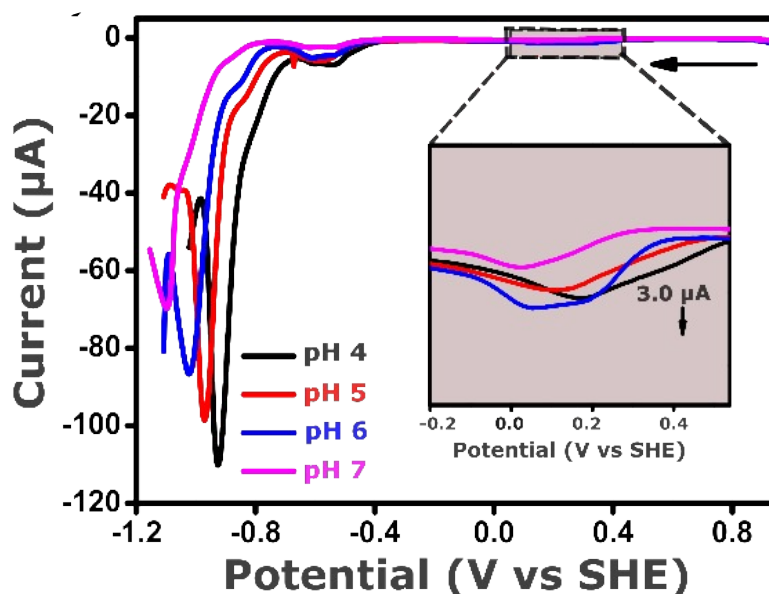

Figure S25. $E_{cat/2}$ and Co^{III}/Co^{II} redox peak of **1** (1 mM) determined by DPV studies in a 0.1 M PBS at different pH. A 3 mm GC working electrode, Pt wire counter electrode, and Ag/AgCl in saturated KCl reference electrode were utilized during the electrochemical measurements. 0.1 M Na_2SO_4 was used as the supporting electrolyte.
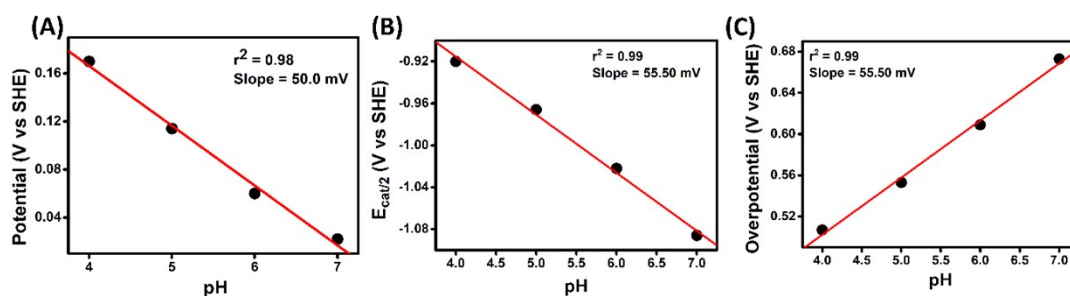
Figure S26. $E_{cat/2}$ and Co^{III}/Co^{II} redox peak and overpotential of **2** (1 mM) determined by DPV studies in a 0.1 M PBS at different pH. Slope 50 mV/pH has extracted for $E_{Co(III/II)}$ and 55.50 mV/pH obtained for $E_{cat/2}$. A 3 mm GC working electrode, Pt wire counter electrode, and Ag/AgCl in saturated KCl reference electrode were utilized during the electrochemical measurements. 0.1 M Na_2SO_4 was used as the supporting electrolyte.
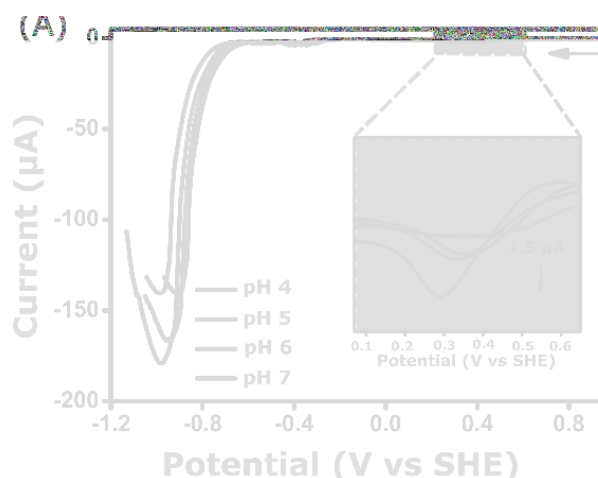

Figure S27. **(A)** $E_{cat/2}$ and Co^{III}/Co^{II} redox peak of **1** (1 mM) determined by DPV studies in a 0.1 M PBS at different pH. **(B)** $E_{cat/2}$ and Co^{III}/Co^{II} redox peak of **1** (1 mM) determined by DPV studies in a 0.1 M PBS at different pH. A 3 mm GC working electrode, Pt wire counter electrode, and Ag/AgCl in saturated KCl reference electrode were utilized during the electrochemical measurements. 0.1 M Na_2SO_4 was used as the supporting electrolyte.
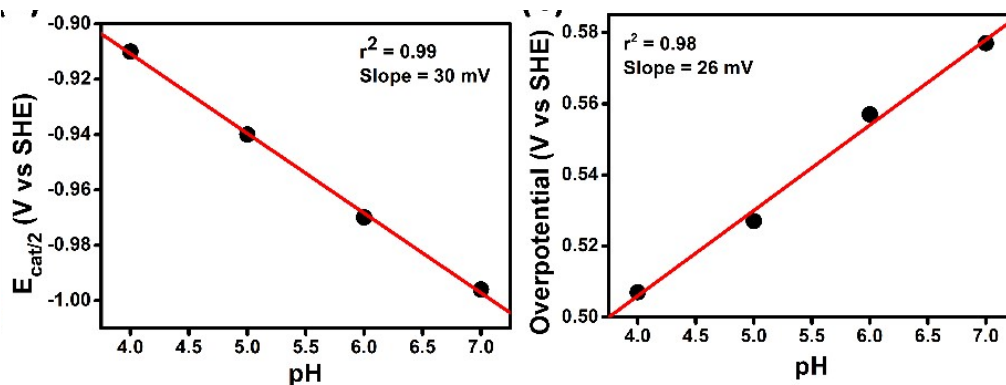

Figure S28. $E_{cat/2}$ and Co^{III}/Co^{II} redox peak and overpotential of **1** (1 mM) determined by DPV studies in a 0.1 M PBS at different pH. Slope 30 mV/pH has extracted for $E_{Co(III/II)}$ and 30 mV/pH obtained for $E_{cat/2}$. A 3 mm GC working electrode, Pt wire counter electrode, and Ag/AgCl in saturated KCl reference electrode were utilized during the electrochemical measurements. 0.1 M Na_2SO_4 was used as the supporting electrolyte.
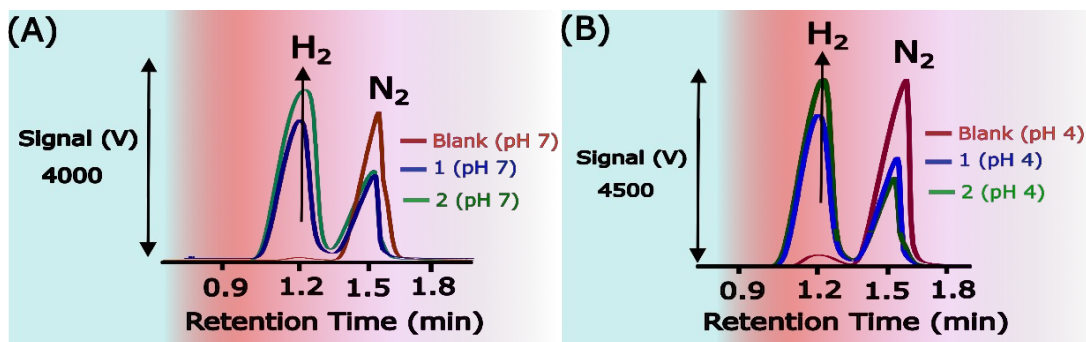
Figure S29. (A) GC data for **1** and **2** at pH 7 along with blank. (B) GC data for **1** and **2** at pH 4 along with blank.

After the CPE (for 2 h) in an H-type cell, a gaseous sample from the headspace of the reaction solution from the compartment containing the working electrode was collected and injected into the GC instrument. A 0.05 mM concentration of the complexes (**1** and **2**) was used for all bulk electrolysis experiments. Applied potential during CPE experiments: pH 7.0. (**1**, −1.15 V vs. SHE; **2**, −1.20 V vs. SHE), pH 4.0. (**1**, −1.15 V vs. SHE; **2**, −1.20 V vs. SHE).
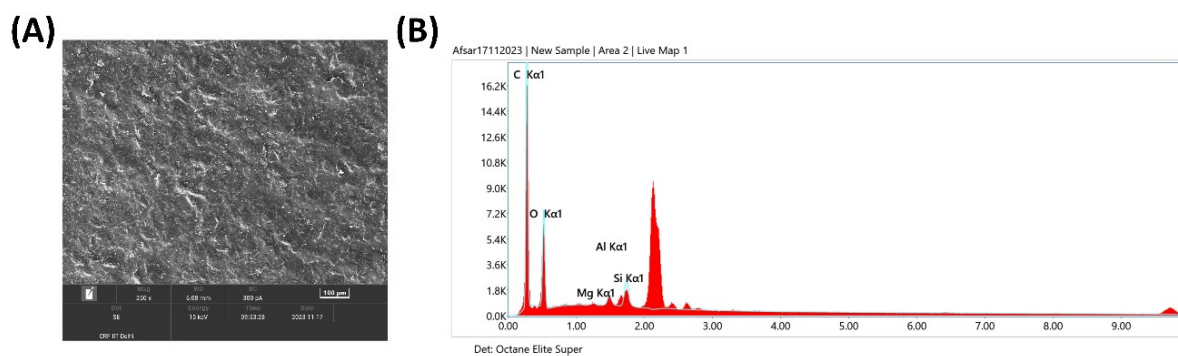

Figure S30. (A) SEM image of the working electrode (plastic chip carbon electrode) after bulk electrolysis experiment (for 2 h) in the presence of **1** (0.05 mM) in a 0.1 M PBS at pH 7.0. (B) EDX image of the working electrode after BE in 0.1 M PBS at pH 7.0.
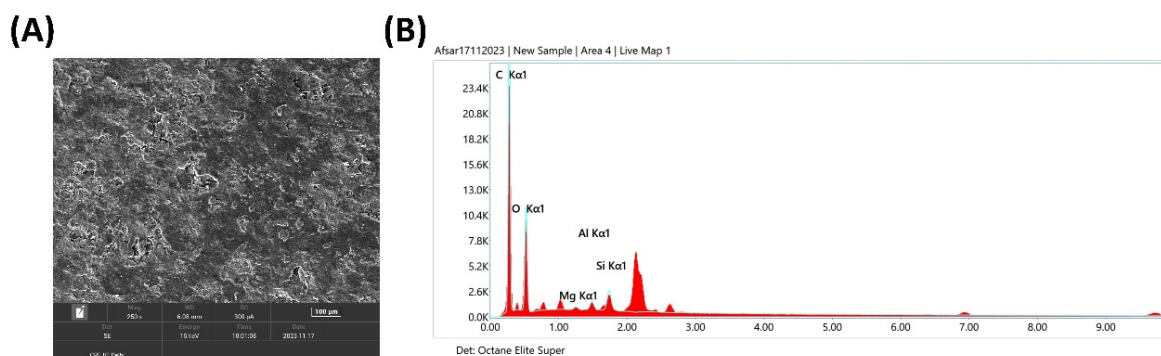

Figure S31. (A) SEM image of the working electrode (plastic chip carbon electrode) after bulk electrolysis experiment (for 2 h) in the presence of **2** (0.05 mM) in a 0.1 M PBS at pH 7.0. (B) EDX image of the working electrode after BE in 0.1 M PBS at pH 7.0.
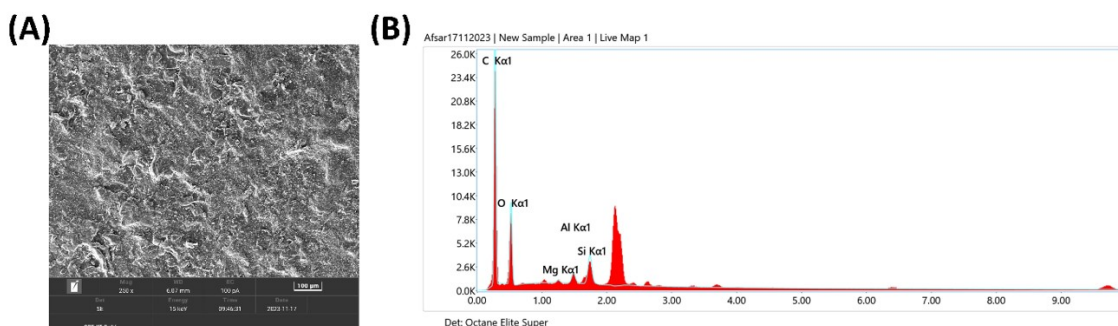
Figure S32. (A) SEM image of the working electrode (plastic chip carbon electrode) after bulk electrolysis experiment (for 2 h) in the presence of **1** (0.05 mM) in a 0.1 M PBS at pH 4.0. (B) EDX image of the working electrode after BE in 0.1 M PBS at pH 4.0.
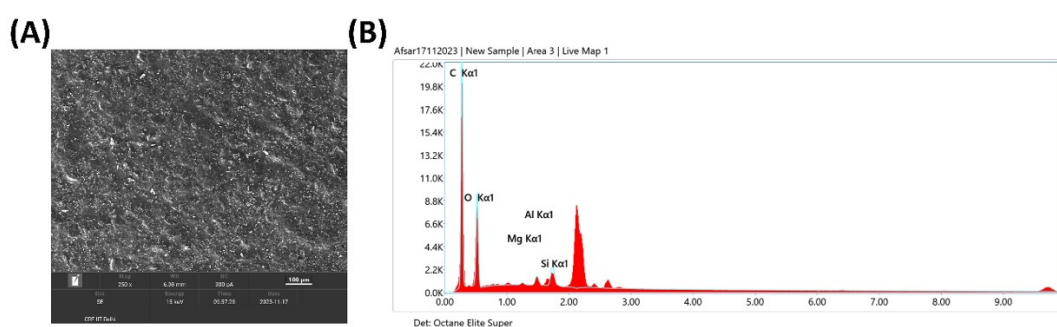

Figure S33. (A) SEM image of the working electrode (plastic chip carbon electrode) after bulk electrolysis experiment (for 2 h) in the presence of **2** (0.05 mM) in a 0.1 M PBS at pH 4.0. (B) EDX image of the working electrode after BE in 0.1 M PBS at pH 4.
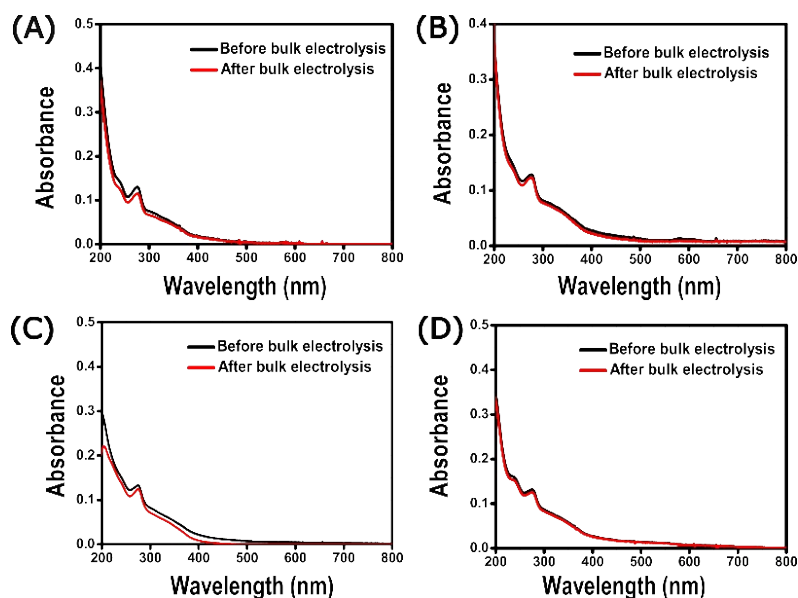

Figure S34. (A) UV spectra recorded before (black trace) and after (red trace) recorded for 1 (0.05 mM) to 2 hr CPE in PBS at pH 4. (B) UV spectra recorded before (black trace) and after (red trace) 2 hr CPE in PBS at pH 7. (C) UV spectra recorded before (black trace) and after (red trace) recorded for 2 (0.05 mM) to 2 hr CPE in PBS at pH 4. (D) UV spectra recorded before (black trace) and after (red trace) 2 hr CPE in PBS at pH 7.
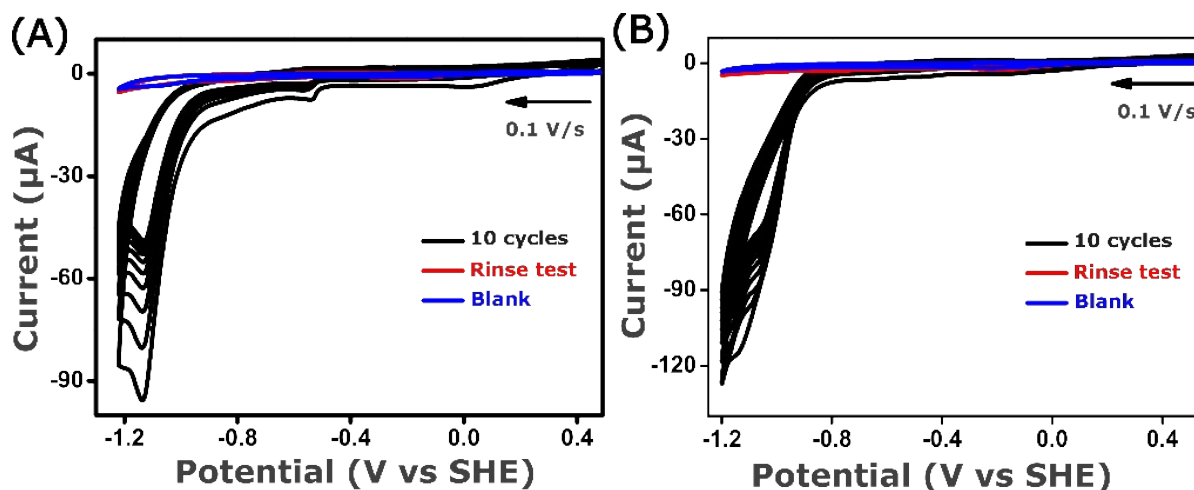
Figure S35. (A) Consecutive CV scans (10 cycles) of **1** in 0.1 M PBS at pH 7.0. After the CV cycles, the working electrode was washed with water, and the CV data (red trace) was taken in a fresh buffer solution using the rinsed working electrode. The blue trace denotes the CV data of a blank 0.1 M PBS buffer solution without the catalyst. (**B**) Consecutive CV scans (10 cycles) of **2** in 0.1 M PBS at pH 7.0. After the CV cycles, the working electrode was washed with water, and the CV data (red trace) was taken in a fresh buffer solution using the rinsed working electrode. The blue trace denotes the CV data of a blank 0.1 M PBS buffer solution without the catalyst. All experiments were measured at 0.1 V/s using a glassy carbon working electrode (3 mm) and Pt wire counter electrode.
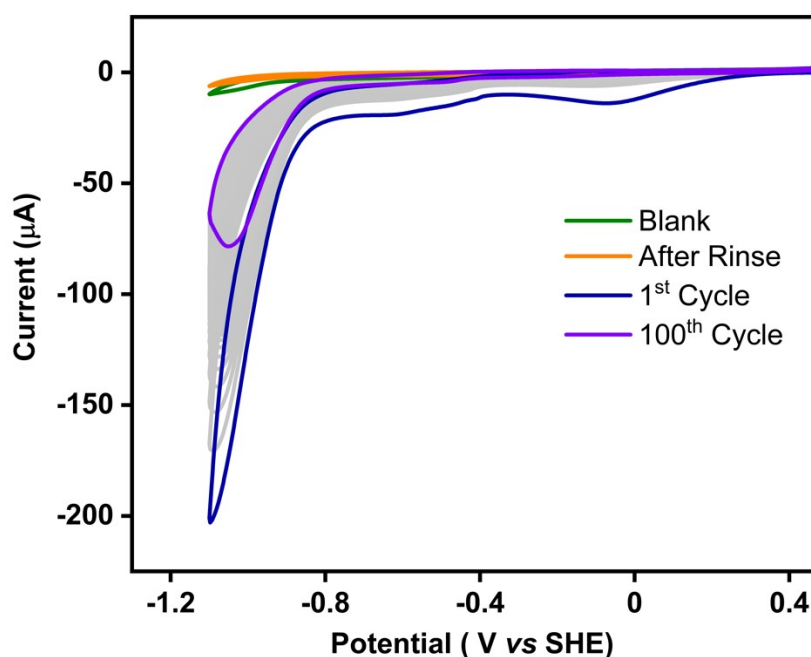

Figure S36. Consecutive CV scans (100 cycles) of **1** in 0.1 M PBS at pH 7.0. After the CV cycles, the working electrode was washed with water, and the CV data was taken in a fresh buffer solution using the rinsed working electrode. The green trace denotes the CV data of a blank 0.1 M PBS buffer solution without the catalyst.
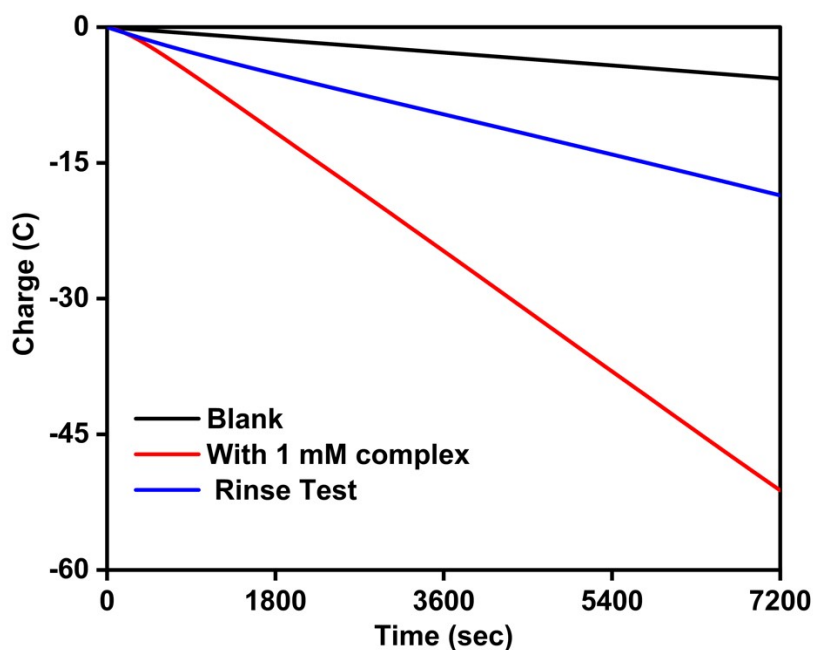
Figure S37. CPE study of **1** (1 mM) in a 0.1 M PBS solution using a PC working electrode (1×1 cm²) at an applied potential of −1.15 V vs. SHE (red trace). After the electrolysis, the working electrode was rinsed with water and subjected to CPE in a fresh 0.1 M PBS at an applied potential of −1.15 V vs. SHE (blue trace). A CPE study using a PC electrode in 0.1 M PBS at Ph 7.0 in the absence of the catalyst is also performed (black trace).
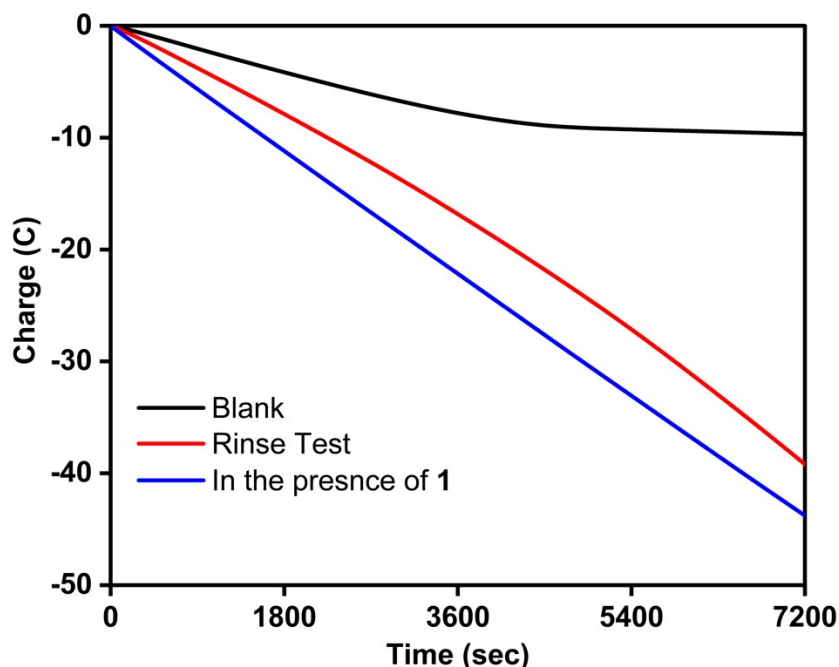

Figure S38. CPE study of **1** (0.05 mM) in a 0.1 M PBS solution using an FTO working electrode (1×1 cm²) at an applied potential of −1.15 V vs. SHE (red trace). After the electrolysis, the working electrode was rinsed with water and subjected to CPE in a fresh 0.1 M PBS at an applied potential of −1.15 V vs. SHE (blue trace). A CPE study using a PC electrode in 0.1 M PBS at pH 7.0 in the absence of the catalyst is also performed (black trace).
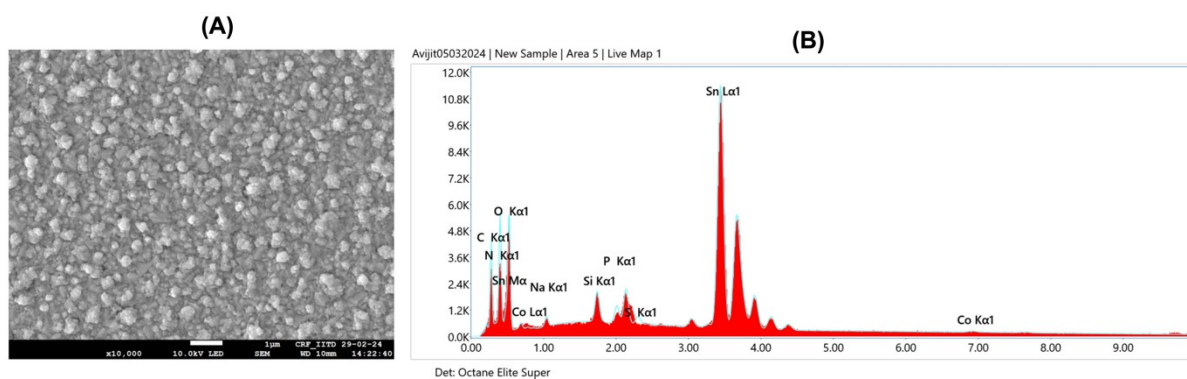
Figure S39. SEM image and EDX data of the FTO working electrode after the CPE experiment at an applied potential of -1.15 V vs. SHE in the presence of **1** (0.05 mM) at pH 7.0. Before the data collection, the WO was washed with deionized water and then dried.

Table S3. EDX data of the FTO working electrode after CPE study in the presence of **1**.

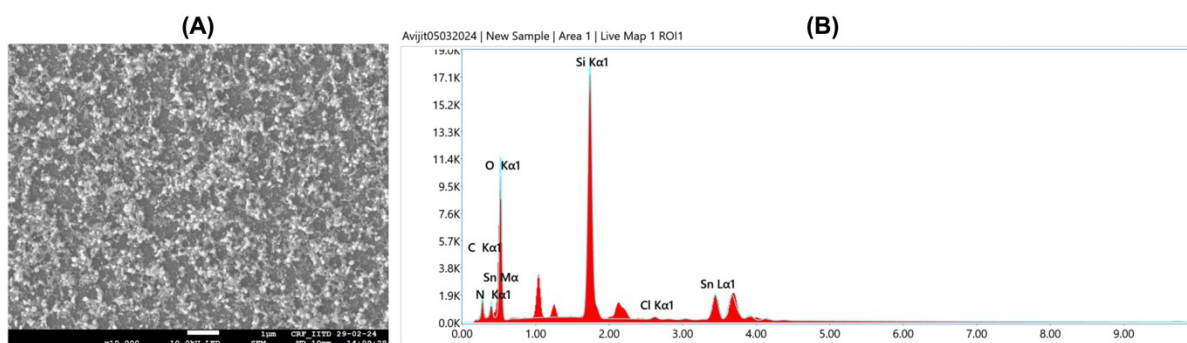| Element	Weight %	
	Blank CPE	CPE with **1**
C K	20.8	11.7
N K	2.8	0.9
O K	33.4	9.7
Na K	-	1.0
Si K	24.5	1.5
P K	-	1.1
S K	-	0.5
Co K	-	0.6
Sn L	18.0	73.1

Figure S40. SEM image (A) and EDX data (B) of the FTO working electrode after the CPE experiment at an applied potential of -1.15 V vs. SHE in the absence of the catalyst at pH 7.0. Before the data collection, the WO was washed with deionized water and then dried.
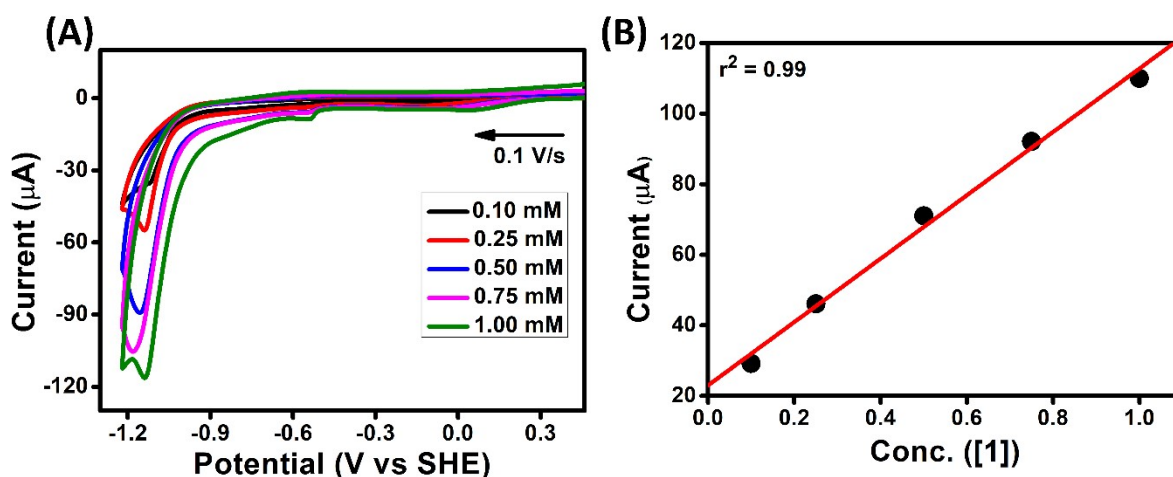
Figure S41. (A) CV data of **1** at variable concentration in a 0.1 M PBS at pH 7, measured at 0.1 V/s scan rate. (B) A plot of catalytic current vs. [**1**] at pH 7.0. A 3 mm GC working electrode, Pt wire counter electrode, and Ag/AgCl in saturated KCl reference electrode were utilized during the electrochemical measurements. 0.1 M Na_2SO_4 was used as the supporting electrolyte.
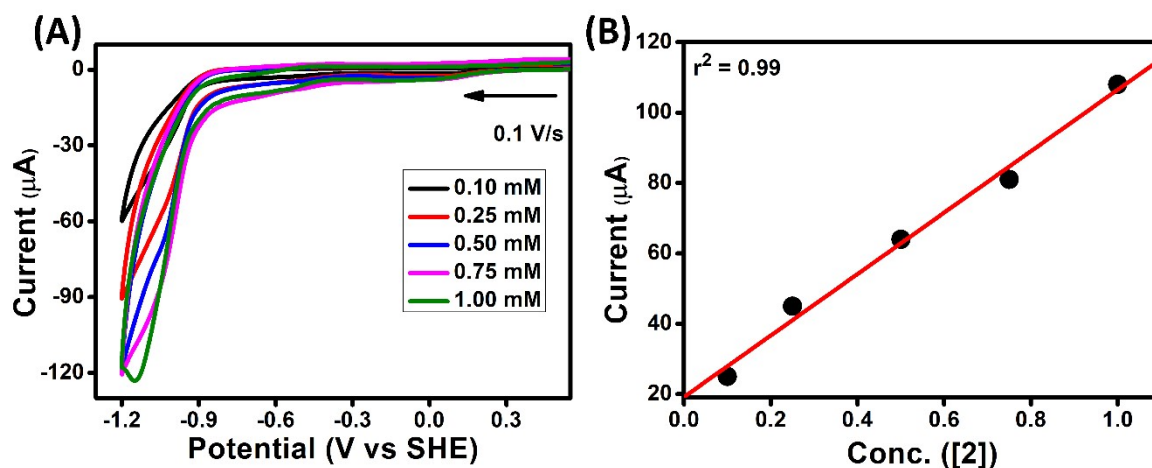

Figure S42. (A) CV data of **2** at variable concentration in a 0.1 M PBS at pH 7, measured at 0.1 V/s scan rate. (B) A plot of catalytic current vs. [**2**] at pH 7.0. A 3 mm GC working electrode, Pt wire counter electrode, and Ag/AgCl in saturated KCl reference electrode were utilized during the electrochemical measurements. 0.1 M Na_2SO_4 was used as the supporting electrolyte.
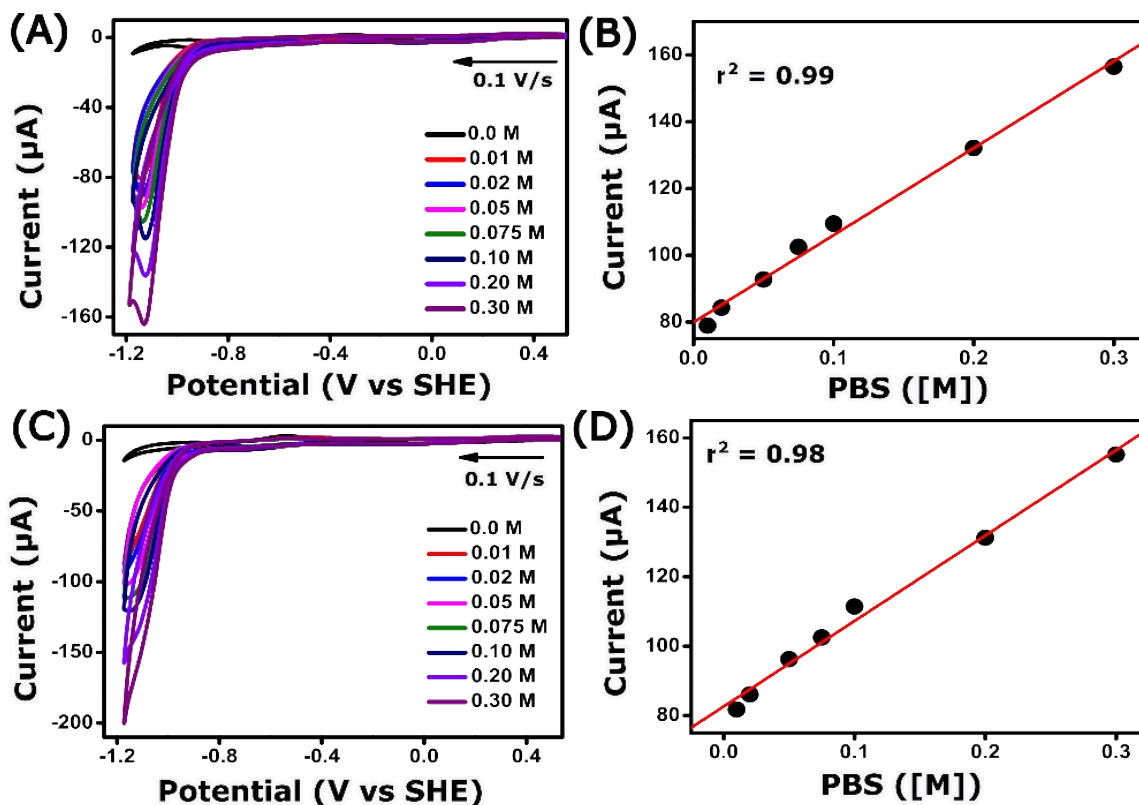
Figure S43. Buffer concentration dependence of **1** (A, 1 mM) and **2** (B, 1 mM) was performed in PBS at pH 7 at variable buffer concentration (0.01 to 0.3 M). Plots C (complex **1**) and D (complex **2**) report a plot of catalytic current vs. buffer concentration (M). A 3 mm glassy carbon working electrode, Pt wire counter electrode, and scan rate of 100 mV/s were used for the measurements.
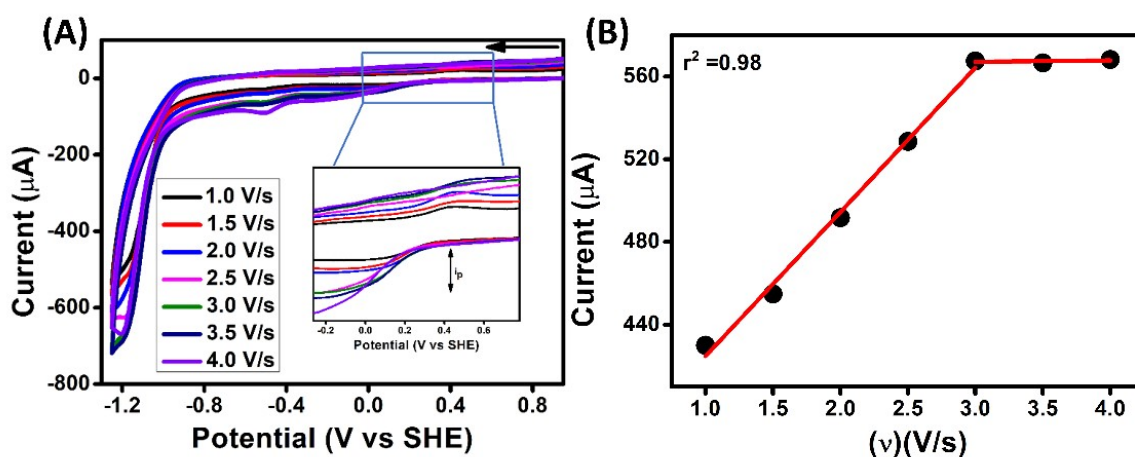

Figure S44. (A) CV data of **1** (1 mM) in a 0.1 M PBS at pH 7, measured at different scan rates (1.0–3.0 V/s). (B) A plot of i_{cat} vs. v for **1** (1 mM). A 3 mm GC working electrode, Pt wire counter electrode, and Ag/AgCl in saturated KCl reference electrode were utilized during the electrochemical measurements. 0.1 M Na_2SO_4 was used as the supporting electrolyte.

Figure S45. (A) CV data of **1** (1 mM) in a 0.1 M PBS at pH 4, measured at different scan rates (1.0–4.0 V/s). (B) A plot of i_{cat} vs. v for **1** (1 mM). A 3 mm GC working electrode, Pt wire counter electrode, and Ag/AgCl in saturated KCl reference electrode were utilized during the electrochemical measurements. 0.1 M Na_2SO_4 was used as the supporting electrolyte.
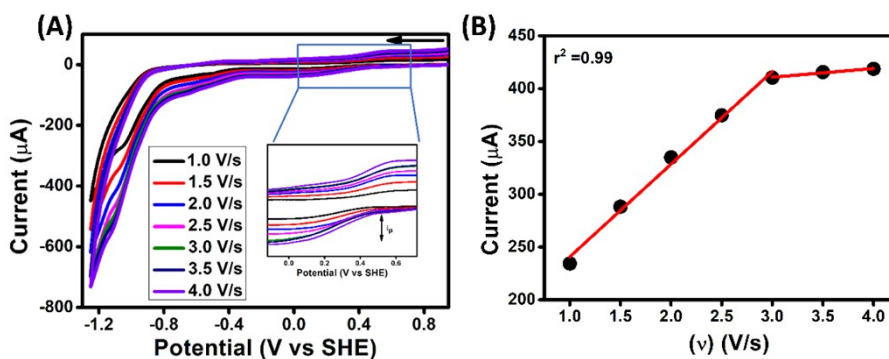

Figure S46. (A) CV data of **2** (1 mM) in a 0.1 M PBS at pH 7, measured at different scan rates (1.0–3.0 V/s). (B) A plot of i_{cat} vs. v for **2** (1 mM). A 3 mm GC working electrode, Pt wire counter electrode, and Ag/AgCl in saturated KCl reference electrode were utilized during the electrochemical measurements. 0.1 M Na_2SO_4 was used as the supporting electrolyte.
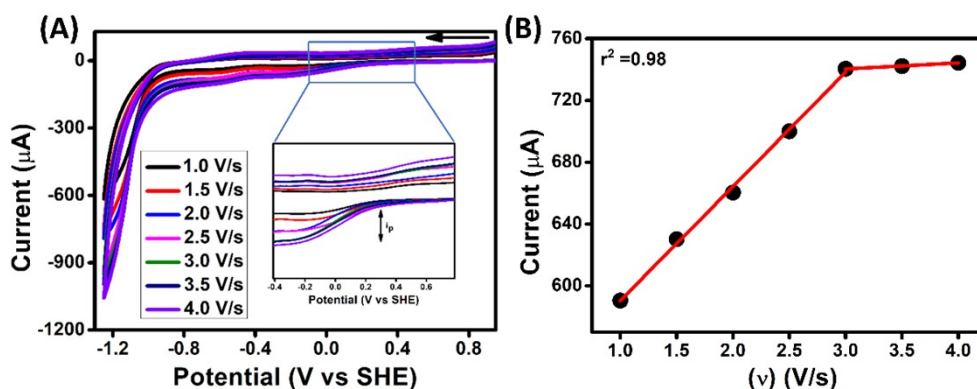

Figure S47. (A) CV data of **2** (1 mM) in a 0.1 M PBS at pH 4, measured at different scan rates (1.0–3.0 V/s). (B) A plot of i_{cat} vs. v for **2** (1 mM). A 3 mm GC working electrode, Pt wire counter electrode, and Ag/AgCl in saturated KCl reference electrode were utilized during the electrochemical measurements. 0.1 M Na_2SO_4 was used as the supporting electrolyte.
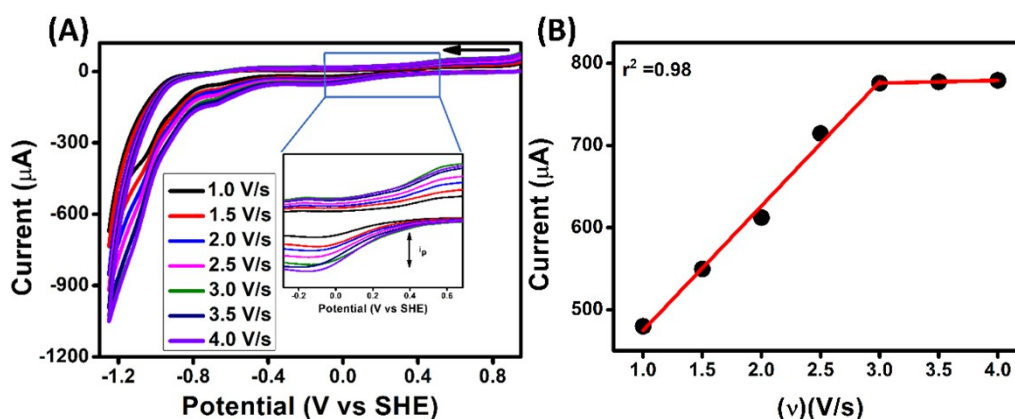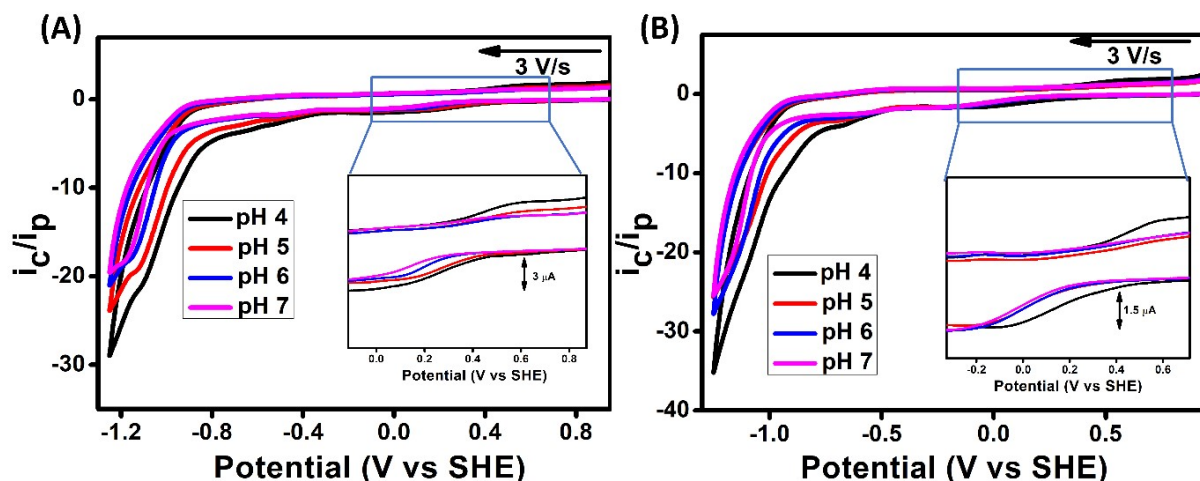
Figure S48. (A) Normalized catalytic current for **1** and **2** at variable pH (4 to 7) in a 0.1 M PBS, measured at 3.0 V/s scan rate. A 3 mm GC working electrode, Pt wire counter electrode, and Ag/AgCl in saturated KCl reference electrode were utilized during the electrochemical measurements. 0.1 M Na_2SO_4 was used as the supporting electrolyte.
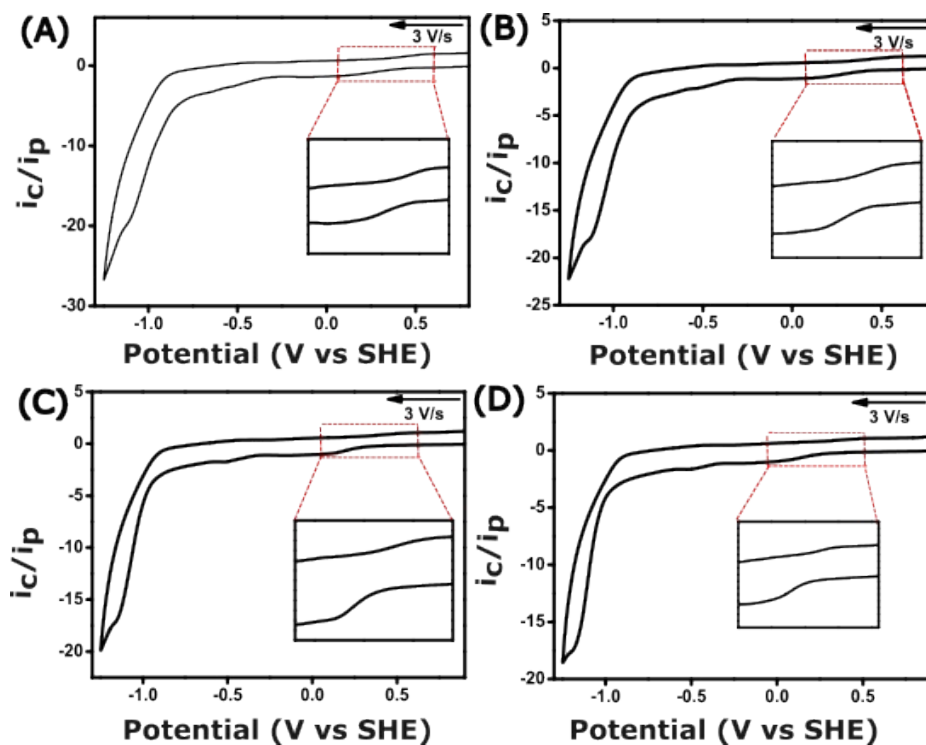

Figure S49. Normalized catalytic current of **1** at pH 4 (A), 5 (B), 6 (C), and 7 (D) in a 0.1 M PBS. The inset data in each of the plots corresponds to the Co^{III}/Co^{II} redox peak. The CV data were recorded at a 3.0 V/s scan rate. A 3 mm GC working electrode, Pt wire counter electrode, and Ag/AgCl in saturated KCl reference electrode were utilized during the electrochemical measurements. 0.1 M Na_2SO_4 was used as the supporting electrolyte.
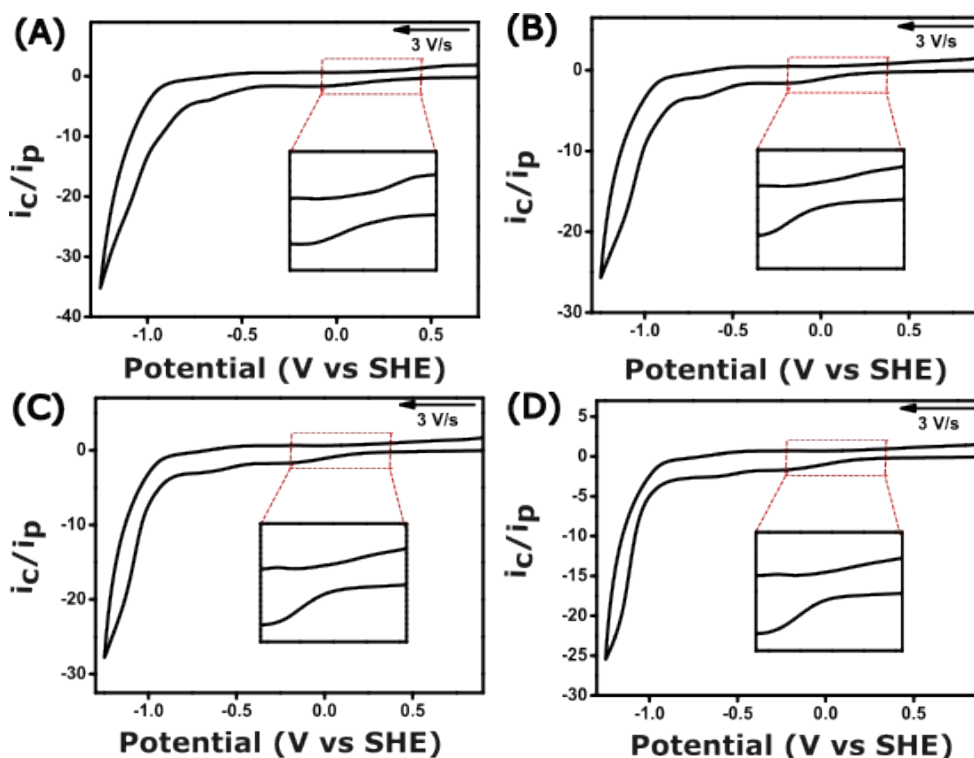
Figure S50. Normalized catalytic current of **2** at pH 4 (A), 5 (B), 6 (C), and 7 (D) in a 0.1 M PBS. The inset data in each of the plots corresponds to the Co^{III}/Co^{II} redox peak. The CV data were recorded at a 3.0 V/s scan rate. A 3 mm GC working electrode, Pt wire counter electrode, and Ag/AgCl in saturated KCl reference electrode were utilized during the electrochemical measurements. 0.1 M Na_2SO_4 was used as the supporting electrolyte.
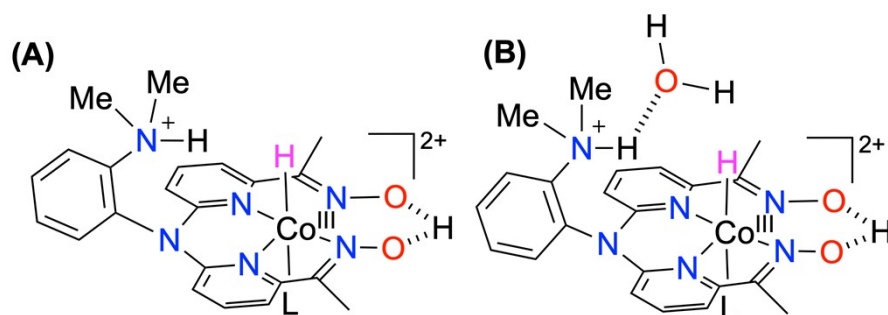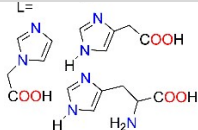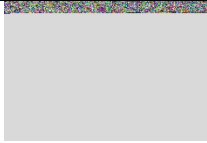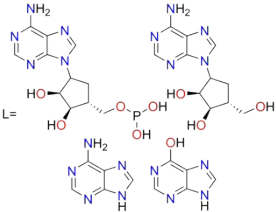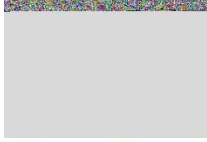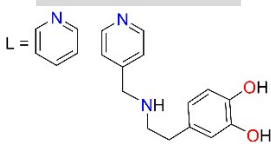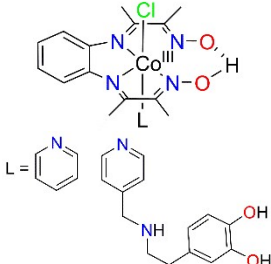

Chart S1. Proposed proton relay during the HER of **2**.

Table S4. A comparison of the catalytic activity of the Co complexes used in this study with the reported Co catalysts.

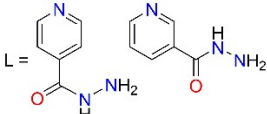| Catalyst	η (mV)	TOF (s^{-1})	TON	Reaction Condition	Reference
	240	–	≈5×10^5 (7h)	Chemically modified GC electrode, Phosphate buffer solution, pH 2, TsOH	4
	782	2.2 h^{-1}	–	pH 2 buffer	5
	787	0.3	–	pH 7, phosphate buffer	6
L = H$_2$O	500 mV	–	23 (2h)	pH 2, phosphate buffer solution	7
	–	–	17 (2h)	pH 2, phosphate buffer solution	7
	241	600	>>10^7	0.5 M H$_2$SO$_4$	8
	565-780 (pH 2) 670-840 (pH 1)	160-190 (pH 2) 255-277 (pH 1)	– –	Aqueous MES buffer solution	9
	505–517 (pH 7) 524–561 (pH 4)	930–8830 (pH 7) 50–850 (pH 4)	–	Aqueous MES buffer solution	10

L= (imidazole/histidine structures)	428–477 (pH 7) 489–503 (pH 4)	3280–4925 (pH 7) 115–328 (pH 4)	–	Aqueous MES buffer solution	[11]
L= (adenosine phosphate structures)	358–395 (pH 7) 304–352 (pH 4)	2040–13300 (pH 7) 200–487 (pH 4)	32-62 (1h)	Aqueous MES buffer solution	[12]
L = (pyridine hydrazide structures)	497 and 498 (pH 7) 489 and 466 (pH 5)	3630 and 2195 (pH 7) 1951 and 794 (pH 5)	–	Aqueous MES buffer solution	[13]
L = (pyridine / dopamine structures)	477 and 467 (pH 7) 534 and 449 (pH 4)	900 and 6370 (pH 7) 150 and 90 (pH 4)	NR and 26.45 (pH 7)	Aqueous MES buffer solution	[14]
L = (Co complex with pyridine / dopamine)	392 and 405 (pH 7) 330 and 514 (pH 4)	200 and 6716 (pH 7) 330 and 514 (pH 4)	4.09 and 16.61 (pH 7)	Aqueous MES buffer solution	[14]
Complex **1**	577 (pH 7) 507 (pH 4)	1300 (pH 7) 1470 (pH 4)	99 (pH 7, 2h) 177 (pH 4, 2h)	Phosphate buffer solution	Present Study
Complex **2**	673 (pH 7) 508 (pH 4)	2630 (pH 7) 4100 (pH 4)	147 (pH 7, 2h) 204 (pH 4, 2h)	Phosphate buffer solution	Present Study

References

1   W. C. Wolsey, *J. Chem. Educ.*, 1973, **50**, A335-A337.
2   G. M. Sheldrick, *Acta Crystallogr., Sect. A Found. Crystallogr.*, 2008, **A64**, 112-122.
3   C. F. Macrae, I. J. Bruno, J. A. Chisholm, P. R. Edgington, P. McCabe, E. Pidcock, L. Rodriguez-Monge, R. Taylor, J. van de Streek and P. A. Wood, *J. Appl. Crystallogr.*, 2008, **41**, 466-470.
4   L. A. Berben and J. C. Peters, *Chem. Commun. (Cambridge, U. K.)*, 2010, **46**, 398-400.
5   B. D. Stubbert, J. C. Peters and H. B. Gray, *J. Am. Chem. Soc.*, 2011, **133**, 18070-18073.
6   Y. Sun, J. P. Bigi, N. A. Piro, M. L. Tang, J. R. Long and C. J. Chang, *J. Am. Chem. Soc.*, 2011, **133**, 9212-9215.
7   C. C. L. McCrory, C. Uyeda and J. C. Peters, *J. Am. Chem. Soc.*, 2012, **134**, 3164-3170.
8   B. Mondal, K. Sengupta, A. Rana, A. Mahammed, M. Botoshansky, S. G. Dey, Z. Gross and A. Dey, *Inorg. Chem.*, 2013, **52**, 3381-3387.
9   S. Khandelwal, A. Zamader, V. Nagayach, D. Dolui, A. Q. Mir and A. Dutta, *ACS Catal.*, 2019, **9**, 2334-2344.
10   D. Dolui, S. Khandelwal, A. Shaik, D. Gaat, V. Thiruvenkatam and A. Dutta, *ACS Catal.*, 2019, **9**, 10115-10125.
11   D. Dolui, S. Das, J. Bharti, S. Kumar, P. Kumar and A. Dutta, *Cell Reports Physical Science*, 2020, **1**, 100007.
12   A. Q. Mir, S. Das, S. Rai, N. A. Shah, P. Majumder and A. Dutta, *ACS Catal.*, 2023, **13**, 8238-8246.
13   G. Afshan, S. Ghorai, S. Rai, A. Pandey, P. Majumder, G. N. Patwari and A. Dutta, *Chem. - Eur. J.*, 2023, **29**, e202203730.
14   S. Ghorai, S. Khandelwal, S. Das, S. Rai, S. Guria, P. Majumder and A. Dutta, *Dalton Trans.*, 2023, **52**, 1518-1523.